Intranasal Human NSC-derived EVs Therapy in Late Middle Age Can Restrain the Activation of NLRP3 Inflammasome and cGAS-STING Signaling in the Aged Hippocampus

Leelavathi N. Madhu[#], Maheedhar Kodali[#], Shama Rao, Sahithi Attaluri, Raghavendra Upadhya[a], Goutham Shankar, Bing Shuai, Yogish Somayaji, Jeswin E. James[a], Padmashri A. Shetty[a], Xiaolan Rao and Ashok K Shetty[§]

 # Contributed equally to this work

Institute for Regenerative Medicine, Department of Cell Biology and Genetics, Texas A&M University College of Medicine, College Station, Texas, USA

Short title: **Neural Stem Cell-Derived EVs Slow Down Hippocampus Aging**

[§]Address of Correspondence:

Ashok K. Shetty, PhD
University Distinguished Professor and Associate Director
Institute for Regenerative Medicine
Department of Cell Biology and Genetics
Texas A&M University School of Medicine,
1114 TAMU, 206 Olsen Boulevard
College Station, TX 77843
E-mail: ash.shetty@tamu.edu

[a]Current address:

Raghavendra Upadhya: Manipal Centre for Biotherapeutics Research, Manipal Academy of Higher Education, Karnataka, Manipal 576104, India.
Jeswin E. James: Department of Molecular and Human Genetics, Baylor College of Medicine, Houston, TX 77030, USA.
Padmashri A. Shetty: Department of Psychiatry, Texas Tech Health, El Paso, TX 79905, USA.

Abstract

Age-related cognitive impairments are linked to detrimental alterations in the hippocampus, which include increased oxidative stress and chronic neuroinflammation known as inflammaging. Inflammaging comprises the activation of the nucleotide-binding domain leucine-rich repeat (NLR) family pyrin domain-containing 3 (NLRP3) inflammasomes, and the cyclic GMP-AMP synthase, and the stimulator of interferon genes (cGAS-STING) pathway that triggers type 1 interferon (IFN-1) signaling. Recent studies have shown that extracellular vesicles from human induced pluripotent stem cell-derived neural stem cells (hiPSC-NSC-EVs) contain therapeutic miRNAs and proteins capable of alleviating oxidative stress and neuroinflammation. This study examined the effects of male and female C57BL6/J mice receiving two doses of intranasal (IN) hiPSC-NSC-EVs (12 x 10^9 EVs/dose, aged-EVs group) or vehicle (aged-Veh group) in late middle age (i.e., at 18 months) on the extent of oxidative stress and chronic neuroinflammation in the hippocampus at 20.5 months of age. Compared to the Aged-Veh group, the hippocampus in the aged-EVs group displayed diminished astrocyte hypertrophy and microglial clusters. Furthermore, the concentrations of oxidative stress markers were reduced, associated with elevated levels of the nuclear factor erythroid 2-related factor 2 and superoxide dismutase and enhanced expression of genes encoding proteins that maintain mitochondrial respiratory chain integrity. Moreover, the hippocampus in the aged-EVs group displayed reduced concentrations of mediators and end products of NLRP3 inflammasome and the downstream p38/mitogen-activated protein kinase activation, and proteins involved in the activation of cGAS-STING-IFN-1 signaling, and the consequent Janus kinase and signal transducer and activator of transcription signaling pathway that leads to the transcription of interferon-stimulated genes. These antioxidant and antiinflammatory molecular changes in the aged-EVs group also improved ability to form recognition and location memories. The results provide the first evidence that IN administrations of hiPSC-NSC-EVs in late middle age can effectively reduce oxidative stress and major neuroinflammatory signaling cascades in the aged hippocampus, leading to better cognitive function in old age.

Keywords: Brain aging, Hippocampus, Inflammasomes, Interferon-1 signaling, Mitochondrial function, Mitogen-activated protein kinase signaling, Neuroinflammation

1. INTRODUCTION

Improved human life expectancy over the past century has brought about longer lives and a surge in age-related ailments. Particularly, neurodegenerative diseases, including Alzheimer's disease (AD), have emerged as the leading causes of morbidity worldwide [1-3]. Hence, effective strategies are urgently needed to promote successful aging, which is characterized by older adults maintaining better cognitive functions, staying engaged in social activities, and displaying minimal signs of age-related diseases [4-6].

Aging is linked to a reduced ability to adapt to new stimuli and cognitive decline in a significant percentage of individuals [7]. Studies using animal models and human post-mortem brain tissues have suggested that cognitive impairments associated with aging are often connected to various adverse changes in the brain, particularly in the hippocampus [6, 8-9]. The age-related changes include increased oxidative stress, mitochondrial dysfunction, and moderate chronic neuroinflammation, which tend to increase substantially in individuals who develop neurodegenerative disorders. Studies have shown that concentrations of oxidative stressors such as reactive oxygen species (ROS) increase gradually during aging, leading to mitochondrial dysfunction [10-11]. Age-related neuroinflammation, also referred to as “inflammaging” is linked to the activation of the nucleotide-binding domain leucine-rich repeat (NLR) family pyrin domain-containing 3 (NLRP3) inflammasomes [12-13] and the cyclic GMP-AMP synthase (cGAS) and the stimulator of interferon genes (STING) pathway, which leads to chronic type I Interferon (IFN) signaling in the aged brain [14].

NLRP3 is predominantly expressed in microglia, the resident immune cells in the brain [15]. Activation of NLRP3 inflammasomes by danger-associated molecular patterns (DAMPs, e.g., increased ROS) in microglia increases the secretion of proinflammatory cytokines, such as interleukin-1 beta (IL-1β) and IL-18. These cytokines can induce pyroptosis in neighboring neural cells and the downstream activation of the p38 mitogen-activated protein kinase (p38/MAPK) signaling pathway via myeloid differentiation primary response 88 (Myd88) and small GTPase rat sarcoma virus (Ras) [12-13, 16-17]. This process can contribute to a chronic state of neuroinflammation with the continuous release of higher concentrations of multiple proinflammatory cytokines. On the other hand, cGAS-STING pathway activation, typically triggered by double-stranded DNA (dsDNA) released from damaged cells, leads to upregulation in the production of type-I IFNs [14, 17] and transcription of interferon-stimulated genes

(ISGs) [14, 18]. Thus, it is apparent that increased oxidative stress, mitochondrial dysfunction, and chronic neuroinflammation in the aged brain increase the susceptibility to develop conditions such as mild cognitive impairment or AD [5, 6, 19]. Therefore, strategies that restrain detrimental inflammatory signaling cascades in the aging brain are needed to maintain better cognitive and mood function in old age. However, treatments capable of restraining such neuropathological changes linked to cognitive and memory impairments in late middle or old age are yet to be identified.

Previous studies have shown some beneficial effects of intracerebral neural stem cell (NSC) grafting in models of brain aging [20-21] and AD [22-23]. However, the benefits of NSC grafting are believed to be primarily due to bystander effects (i.e., paracrine actions of their secretome), which include antiinflammatory, neuroprotective, and neuroreparative activity [24-25]. From this perspective, extracellular vesicles (EVs) from human induced pluripotent stem cell (hiPSC)-derived NSCs, retaining most of the therapeutic effects of parental cells, have attracted attention in developing cell-free therapies. Also, intranasally (IN) administered hiPSC-NSC-EVs efficiently target microglia and astrocytes mediating neuroinflammation in the entire brain [26-27] and has been shown to induce beneficial transcriptomic changes in conditions such as AD [17]. Furthermore, the cargo (miRNAs and proteins) carried by these EVs have been validated earlier for their competence to mediate antiapoptotic, antiinflammatory and neuroprotective effects using *in vitro* and *in vivo* models [17, 26, 28-30]. Therefore, using a mouse model, this study investigated the proficiency of IN administration of hiPSC-NSC-EVs as an anti-aging therapy in late middle age to maintain better cognitive function in old age. The results provide new evidence that hiPSC-NSC-EVs administration in late middle age can reduce oxidative stress and mitochondrial dysfunction, restrain the activation of NLRP3 and cGAS-STING signaling pathways, and maintain better cognitive and mood function in old age.

2. MATERIALS AND METHODS

2.1. hiPSC-derived NSC cultures, purification and characterization of hiPSC-NSC-EVs

The procedures for generating NSCs from hiPSCs, passaging of hiPSC-NSCs, isolation of EVs from passage 11 (P11) hiPSC-NSCs, and characterization of the number, size, and markers of hiPSC-NSC-EVs are detailed in our previous reports [17, 26, 28] and the supplemental file.

2.2. Animals and Study Design

The study comprised two cohorts of C57BL/6 mice: young adult (3 months old) and late middle-aged (18 months old). The mice were purchased from Jackson Laboratories (Bar Harbor, Maine, USA) and were housed with ad libitum access to food (with a 4% fat diet) and water (n=125, 59 males and 66 females). The institutional animal care and use committee of Texas A&M University approved all studies performed in this investigation. Male and female late middle-aged mice were randomly assigned to either the vehicle group (aged-Veh; n=31 [13 males and 18 females]) or the EVs group (aged-EVs; n=30 [12 males; 18 females]). Furthermore, additional groups of 3-month-old mice (n=28, 14 males and 14 females) and 18-month-old mice (n=32, 16 males and 16 females) underwent neurobehavioral studies to determine the cognitive status at 18 months of age, the timepoint chosen for hiPSC-NSC-EVs treatment intervention in the study. Additional late middle-aged mice (n=4, males) were used to evaluate the incorporation of IN-administered PKH-26-labeled hiPSC-NSC-EVs into neural cells across various brain regions. Figure 1 [E, H] details the study design, including the time points for the IN-administration of hiPSC-NSC-EVs, neurobehavioral tests, and euthanasia.

The animals in the aged-Veh or aged-EVs group received two doses of the vehicle or the hiPSC-NSC-EVs (12×10^9 EVs) treatment, with each dose administered two weeks apart. One month after the last dose, the animals in all groups were subjected to neurobehavioral tests. Following cognitive assessments, subgroups of animals were perfused with 4% paraformaldehyde, and collected brain tissues were processed for immunohistochemical studies (n=6-8/group) or euthanized to harvest fresh brain tissues for biochemical and molecular biological studies (n=6-8/group). The investigators conducting the behavioral tests and those performing immunohistochemical, immunofluorescence, biochemical, or molecular biological analyses were blinded to the group identities of animals or samples. An additional cohort of late middle-aged male mice (n=4) received IN administration of hiPSC-NSC-EVs labeled with PKH-26 dye (4×10^9 EVs) were euthanized 6 hours after EVs administration to confirm the biodistribution of EVs into neural cells across various regions of the brain.

2.3. Evaluation of the interaction of IN-administered hiPSC-NSC-EVs with microglia and astrocytes

The animals were perfused with 4% paraformaldehyde six hours after an IN administration of PKH-26-labeled hiPSC-NSC-EVs to visualize the interaction of IN-administered PKH-26-labeled hiPSC-

NSC-EVs (fluorescing red) with neural cells. Thirty micrometer thick serial sections were cut using a cryostat, and every 15th section through the entire forebrain from each animal (n=4) was processed for ionized calcium-binding adaptor molecule 1 (IBA-1) or glial fibrillary acidic protein (GFAP) immunofluorescence to confirm the interaction or association of PKH-26-labeled hiPSC-NSC-EVs with microglia and astrocytes. The primary and secondary antibodies comprised anti-goat IBA-1 (1:1000, Abcam), rabbit anti-GFAP (1:2000, Dako), donkey anti-goat IgG tagged with Alexa Fluor 488 (1:200, Invitrogen), and donkey anti-rabbit IgG tagged with Alexa Flour 488 (1:200, Invitrogen). The supplemental file comprises the methods employed for IBA-1 and GFAP immunofluorescence.

2.4. Analyses of cognitive function

The study employed two neurobehavioral tests to measure cognitive function. A novel object recognition test (NORT) was used to investigate the competence for recognition memory, which relies on an interaction between the hippocampus and the perirhinal cortex [31]. Furthermore, an object location test (OLT) investigated the proficiency of animals to discern subtle changes in their immediate environment, a cognitive function dependent on the integrity of the hippocampus [32]. The detailed protocols utilized for NORT and OLT are available in our previous reports [16-17, 33-34] and the supplementary file. In animals receiving vehicle or hiPSC-NSC-EVs treatment, these tests were performed between 19.5 and 20.5 months of age, along with age-matched naïve control animals.

2.5. Tissue processing, and immunohistochemical, immunofluorescence, and biochemical studies

After the completion of cognitive tests (i.e., at 20.5 months of age), the animals were euthanized, and the brain tissues were processed for immunohistochemical and biochemical analyses. The detailed methods employed for brain tissue collection, processing, immunohistochemistry, single/dual/triple immunofluorescence, and biochemical and molecular biological studies are available in our previous reports [16-17, 35-36] and the supplemental file.

2.6. Quantification of number and clusters of microglia in the hippocampus

The microglial clusters and microglial numbers in the hippocampus of male and female mice belonging to aged-Veh and aged-EVs groups (n=6/group) were measured, using every 20th section

through the hippocampus. Microglial numbers were measured via stereological counting of IBA1+ cells using the optical fractionator method in the StereoInvestigator system (Microbrightfield, Williston, Vermont, USA). They were expressed as the number per 0.1 mm^3 volume of the hippocampus. The detailed stereological methods employed are described in our earlier reports [37-39]. We quantified the total number of microglial clusters for the hippocampus by counting the number of clusters in serial sections (every 20th) through the entire hippocampus and extrapolating the average number per section with the total number of sections through the hippocampus (n=5-6/group).

2.7. Measurement of oxidative stress markers, antioxidants, and nuclear factor erythroid 2-related factor 2 (NRF2)

Commercially available kits were employed to measure oxidative stress markers malondialdehyde (MDA) and protein carbonyls (PC) (Cayman Chemicals, Arbor, MI), and NRF2 (Signosis, Santa Clara, CA), in hippocampal lysates. We followed the manufacturer's instructions for performing these assays. Furthermore, to evaluate the status of antioxidants in the hippocampus, we measured superoxide dismutase (SOD) and catalase (CAT) concentrations in hippocampal lysates. The total protein concentration in the various tissue lysates was determined using a Pierce BCA reagent kit from Thermo Fisher Scientific (Waltham, MA). The concentrations of markers were normalized to the total protein content in their respective tissue lysates.

2.8. Measurement of genes linked to mitochondrial respiratory chain

We analyzed the expression of many genes regulating the mitochondrial respiratory chain in the hippocampus, using specific primers purchased from Genecopoeia (Rockville, MD) (n=6/group). The measured genes encoding proteins relevant to the mitochondrial electron transport chain and oxidative phosphorylation include the NADH: ubiquinone oxidoreductase subunit S6 and S7 (Ndufs6 and Ndufs7 - complex I), succinate dehydrogenase A and B (SdhA and SdhB - complex II), BCS1 homolog, ubiquinol-cytochrome C reductase complex chaperone (Bcs1l - Complex III) and cytochrome C1 (Cyc1 - complex III); Cytochrome c oxidase subunit 6a (Cox6a - complex IV) and cytochrome C oxidase subunit 4i2 (Cox4i2 - complex IV) and cytochrome c oxidase subunit 7B (Cox7b-Complex IV)), ATPase H+ transporting accessory protein 1 (Atp6ap1 - complex V), and Solute Carrier Family 25 Member 10 (Slc25a10 - mitochondrial membrane transporter). Glyceraldehyde 3-phosphate dehydrogenase (Gapdh) was used

as a housekeeping gene. The 2^delta-delta Ct (2^{ddCT}) values for each gene were compared across different groups.

2.9. Measurement of NLRP3 inflammasome genes, and NLRP3-ASC inflammasome complexes in microglia

We first performed qRT-PCR to measure the expression of genes Nlrp3, Pycard, Casp1, Il1b, and Il18. Then, to determine the extent of NLRP3-apoptosis-associated speck-like protein containing a caspase recruitment domain (ASC) inflammasome complexes and the percentages of microglia presenting NLRP3-ASC complexes, the brain tissue sections were processed for triple immunofluorescence to visualize IBA-1, NLRP3, and ASC in microglia. Using Z-section analysis in a Nikon confocal microscope or a Leica THUNDER 3D Imager (3 images/section, three sections/animal, n=6 animals/group), the number of NLRP3-ASC inflammasome complexes per unit area (~216 µm2) and the percentages of IBA-1+ microglia co-expressing NLRP3-ASC inflammasome complexes were measured. For these quantifications, data collected from individual subfields (DG, CA1, and CA3) of the hippocampus were pooled (3 sections/animal, n=6/group) [16-17, 29]. The supplemental file comprises information on the antibodies and detailed methods.

2.10. Quantification of markers involved in the activation of NLRP3 inflammasome and p38/MAPK signaling cascades

The hippocampal lysates from male and female mice were processed to quantify the concentrations of the various markers of NLRP3 inflammasome activation and p38/MAPK signaling (n=6/group), using commercially available individual enzyme-linked immunoassay (ELISA) kits, as detailed in our previous studies [16-17, 40]. These include assay kits for 1) nuclear subunit of Nuclear factor kappa B (NF-kB p65; Aviva Systems Biology, San Diego, CA, USA), 2) NLRP3 (Abcam, Cambridge, MA, USA), 3) ASC (MyBioSource, San Diego, CA, USA), 4) cleaved caspase-1 (Abcam), 5) IL-18 (R&D Systems, Minneapolis, MN, USA), 6) IL-1β (R&D Systems, 7) MyD88 (Aviva Systems Biology), 8) Ras, (MyBioSource), 9) p38 MAPK (Cell Signaling, Danvers, MA, USA), 10) activator protein-1 (AP-1, Novus Biologicals, Centennial, CO; USA), and 11) tumor necrosis factor-alpha (TNF-α, R&D systems), and 12) IL-8 (Biomatik, Wilmington, DE, USA). The concentrations of individual proteins were normalized to the 1 mg of total protein in hippocampal lysates.

2.11. Quantification of markers associated with activation of cGAS-STING signaling pathway

We measured the concentrations of 1) c-GAS (Cell Signaling, Danvers, Massachusetts, MA), 2) p-STING(Cell signaling), 3) phosphorylated TANK-binding kinase-1 (p-TBK-1), 4) phosphorylated interferon regulatory factor 3 (p-IRF3; Abclonal, Woburn, Massachusetts MA), and 5) IFN-α (LS-BIO, Lynnwood, WA) in hippocampal lysates of male and female mice [17]. Since the activation of the cGAS-STING pathway stimulates the JAK-STAT signaling [41], we also measured concentrations of the phosphorylated JAK1 and JAK2 and the phosphorylated STAT1 and STAT3 in the hippocampal lysates of male and female aged mice.

2.12. Statistical analyses

Statistical analyses were done using Prism software version 10.2. Within-group comparisons in neurobehavioral tests and two-group comparisons utilized either a two-tailed, unpaired Student's t-test or a Mann-Whitney U-test, depending on whether the datasets had significantly different standard deviations. A p-value of less than 0.05 was considered statistically significant in all tests. A two-way ANOVA followed by Tukey's multiple comparisons post-hoc tests were employed to assess sex-dependent effects and the interaction between sex and hiPSC-NSC-EVs treatment.

3. RESULTS

3.1. Attributes of hiPSC-NSC-EVs employed in the study

The P11 hiPSC-NSC cultures employed in the study exclusively comprised NSCs, as all cells expressed the NSC markers nestin and Sox-2 (Fig. 1 [A]). EVs isolated from these cultures by anion-exchange and size-exclusion chromatographic techniques had a mean size of 130.9 nm (Fig. 1 [B]). These EVs exhibited specific markers, such as the tetraspanins CD63 and CD81, and ALIX. However, they did not contain the cytoplasmic marker calnexin, which is present in hiPSC-NSCs (Fig. 1 [C]). Additionally, transmission electron microscopy confirmed the presence of double-membrane-bound vesicles in the EV preparations (Fig. 1 [D]). Our previous study has demonstrated that various protein and miRNA cargo

carried by these hiPSC-NSC-derived EVs have antioxidant, antiinflammatory, and neuroprotective properties [26, 28].

3.2. Biodistribution of IN-administered hiPSC-NSC-EVs in the brain of late middle-aged mice

The biodistribution of IN-administered PKH-26-labeled hiPSC-NSC-EVs (4 x 10^9 EVs) was examined in multiple brain regions using markers of neural cells at 6 hours post-administration (Fig. 1 [E]). Such analysis revealed that hiPSC-NSC-EVs permeated virtually all brain regions within six hours post-administration, as demonstrated in our earlier studies for naïve mice [26] and 5x Familial AD (5xFAD) mice [27]. In all brain regions, these EVs are taken up by microglia and neurons and were also seen in contact with the cell membranes of astrocytes and oligodendrocytes. As this study focused on hiPSC-NSC-EVs treatment-mediated changes in microglia and astrocytes, examples of hiPSC-NSC-EVs incorporation by IBA-1+ microglia and the interaction of hiPSC-NSC-EVs with the plasma membrane of soma and processes of GFAP+ astrocytes in the hippocampal subregions (DG, CA1, and CA3) are illustrated (Fig. 1 [F-G]). Overall, the biodistribution of IN-administered hiPSC-NSC-EVs in late middle-aged mice mirrored the distribution pattern observed in young adult mice [26-27].

[Figure 1 here]

3.3. hiPSC-NSC-EVs reduced astrocyte hypertrophy in the hippocampus

An evaluation of the morphology of GFAP+ astrocytes in the hippocampus suggested that hypertrophy of astrocytes decreased in the aged-EVs group compared to the aged-Veh group. Representative images from the CA3 subfield of the hippocampus from male and female aged-Veh and aged-EVs groups are illustrated (Fig. 2 [A-D]). Measurements of the area fraction of GFAP+ astrocytic elements in the hippocampus, using ImageJ, confirmed that both male and female subjects in the aged-EVs group exhibited lower levels of GFAP+ structures than their counterparts in the aged-Veh group ($p<0.0001$; Fig. 2 [E-F]). A two-way ANOVA analysis revealed sex-dependent differences in astrocyte hypertrophy within the aged-Veh group, with the male mice exhibiting higher levels of astrocyte hypertrophy than female mice ($p<0.05$). However, an analysis of the interaction between sex and EVs treatment demonstrated that both male and female mice responded positively to EVs treatment

($p<0.05$; Suppl. Table 1). Thus, treatment with hiPSC-NSC-EVs in late middle age can reduce astrocyte hypertrophy in the aged hippocampus.

[Figure 2 here]

3.4. hiPSC-NSC-EVs reduced microglial numbers and clusters in the hippocampus

Analysis of the distribution of IBA-1+ microglia in the hippocampus suggested a comparable density of microglia in the aged-EVs group compared to the aged-Veh group. Representative images from the CA3 subfield of the hippocampus from male and female aged-Veh and aged-EVs groups are illustrated (Fig 2 [G-J]). Stereological quantification of the microglial numbers per unit volume of the hippocampus confirmed that both male and female mice from the aged-Veh and aged-EVs group displayed comparable densities of IBA-1+ microglia in the hippocampus ($p>0.05$; Fig. 2 [K-L]) implying that EVs treatment did not alter the microglial number. However, an examination of microglial clusters comprising hypertrophied microglia indicating disease-associated microglia phenotypes [42-43] in the hippocampus revealed reduced frequency in the aged-EVs group than the aged-Veh group. Representative examples from the dentate molecular layer of male and female mice belonging to aged-Veh and aged-EVs groups are illustrated (Fig. 2 [M-P]). Quantification of these microglial clusters along the septo-temporal axis of the hippocampus confirmed that both male and female mice in the aged-EVs group had fewer microglial clusters compared to those in the aged-Veh group ($p<0.01$-0.001, Fig. 2 [Q-R]). A two-way ANOVA analysis revealed neither sex-dependent differences in microglial numbers or clusters in aged-Veh and aged-EVs groups nor interactions between sex and hiPSC-NSC-EVs treatment (Suppl. Table 1). Thus, hiPSC-NSC-EVs treatment in late middle age can reduce disease-associated microglia phenotypes in the aged hippocampus.

3.5. hiPSC-NSC-EVs reduced oxidative stress with enhanced NRF2 in the hippocampus

Proficiency of hiPSC-NSC-EVs to reduce oxidative stress was investigated by measuring markers of oxidative stress (MDA and PCs), the master regulator of oxidative stress (NRF2), and antioxidants (SOD and CAT). Compared to the aged-Veh group, both males and females in the aged-EVs group displayed reduced concentrations of MDA and PCs ($p<0.01$-0.0001, Fig. 3 [A-B, F-G]), increased concentrations of NRF-2 and SOD ($p<0.01$, Fig. 3 [C-D, H-I]). The concentration of CAT in the aged-EVs

group was increased in females ($p<0.01$, Fig. 3 [J]) but not in males ($p>0.05$, Fig. 3 [E]). Two-way ANOVA analyses showed neither sex-dependent differences in the concentrations of MDA, PCs, NRF2, and SOD in aged-Veh and aged-EVs groups nor interactions between sex and hiPSC-NSC-EVs treatment. However, catalase concentration was sex-dependent in the aged-EVs group, with females exhibiting an increased concentration ($p<0.01$, Suppl Table 1), and interaction between sex and EVs treatment revealed that only female mice responded positively to EVs treatment ($p<0.01$; Suppl Table 1). Thus, hiPSC-NSC-EVs treatment in late middle age can reduce oxidative stress in the aged hippocampus.

3.6. hiPSC-NSC-EVs enhanced mitochondrial respiratory chain gene expression in the hippocampus

The competence of hiPSC-NSC-EVs to enhance the expression of genes linked to the mitochondrial respiratory chain was investigated in the hippocampus since increased oxidative stress damages mitochondria, leading to an impaired mitochondrial respiratory chain activity [44]. The measured genes comprised those linked to the activity of complex I (Ndufs6, Ndufs7), complex II (Sdha, Sdhb), complex III (Cyc1, Bcs1l), complex IV (Cox7b, Cox4i2), and complex V (Slc25a1, Atp6ap1) (Fig. 3 [K, V]). Compared to the aged-Veh group, males in the aged-EVs group displayed significantly increased expression of many genes, including Ndufs6, Ndufs7, Sdha, Sdhb, Cyc1, Cox4i2, Slc25a1, and Atp6ap1 ($p<0.05$-0.01, Fig. 3 [L-P, S-U]). Females in the aged-EVs groups showed a similar trend but with fewer genes (Ndufs6, Ndufs7, Cyc1, Cox4i2, Slc25a1) showing significantly increased expression than their counterparts in the aged-Veh group ($p<0.05$-0.001, Fig. 3 [W-X, AA, AD-AE]). Two-way ANOVA analyses showed neither sex-dependent differences in aged-Veh and aged-EVs groups nor interactions between sex and hiPSC-NSC-EVs treatment for most of the measured genes linked to the mitochondrial respiratory chain ($p>0.05$, Suppl. Table 1). However, the expression of Ndufs6 was sex-dependent in the aged-EVs group, with females exhibiting an increased expression ($p<0.05$, Suppl Table 1), but analysis of the interaction between sex and EVs treatment revealed that Nduf6 expression in both male and female mice responded positively to EVs treatment ($p<0.01$; Suppl Table 1). Thus, hiPSC-NSC-EVs treatment in late middle-aged male and female mice enhanced mitochondrial respiratory chain gene expression in the aged hippocampus.

[Figure 3 here]

3.7. hiPSC-NSC-EVs restrained the activation of NLRP3 inflammasome cascade in the hippocampus

Proficiency of hiPSC-NSC-EVs to restrain the activation of NLRP3 inflammasomes was examined by three measures, which include quantification of 1) the expression of associated genes such as NLRP3, PYCARD/ASC, CASP1, IL-18 and IL-1β (Fig. 4 [A-L]), 2) percentages of microglia exhibiting NLRP3-ASC complexes (Fig. 4 [M-Z]) and 3) the concentrations of proteins involved in their activation including NF-kB-p65, NLRP3, ASC, Cleaved Caspase-1, IL-18, IL-1β, (Fig. 4 [AA-AL]). Compared to the aged-Veh group, males in the aged-EVs group displayed decreased expression of all measured genes, with NLRP3, ASC, and IL-18 showing a significant decline ($p<0.05$-0.001, Fig. 4 [B-C, E]). Females in the aged-EVs groups showed a similar trend, with NLRP3 and IL-18 showing a significantly decreased expression than their counterparts in the aged-Veh group ($p<0.05$, Fig. 4 [H, K]). Next, the extent of NLRP3-ASC inflammasome complexes within microglia of the hippocampus was examined via triple immunofluorescence for NLRP3, ASC, and IBA-1 and Z-section analysis (Fig. 4 [M-Y]). In comparison to the aged-Veh group, both males and females in the aged-EVs group displayed decreased percentages of microglia exhibiting NLRP3-ASC inflammasome complexes ($p<0.01$, Fig. 4 [S, Z]).

To corroborate the above findings, the concentrations of proteins involved in NLRP3 inflammasome activation were measured. Compared to the aged-Veh group, males in the aged-EVs group displayed decreased concentrations of all measured proteins, with NF-kB-p65, NLRP3, ASC, and IL-18 showing a significant decline ($p<0.05$-0.001, Fig. 4 [AA-AC, AE]). Females in the aged-EVs groups showed a similar trend with NLRP3, ASC, Cleaved Caspase-1, IL-18 and IL-1β showing significantly decreased concentrations than their counterparts in the aged-Veh group ($p<0.05$-0.0001, Fig. 4 [AH-AL]). Two-way ANOVA analyses showed neither sex-dependent differences in Aged-Veh and aged-EVs groups nor interactions between sex and hiPSC-NSC-EVs treatment for all measured genes and a vast majority of the measured proteins linked to NLRP3 inflammasome activation ($p>0.05$, Suppl. Table 1). The exception is the concentration of NLRP3, which showed an interaction between sex and EVs treatment although both males and females responded positively to EVs treatment ($p<0.05$; Suppl Table 1). Thus, hiPSC-NSC-EV treatment in late middle-aged male and female mice significantly inhibited the activation of NLRP3-ASC inflammasomes in the aged hippocampus. Such effect was evident from reduced concentrations of 1) the transcription factor NF-kB-p65 that triggers the formation of NLRP3 inflammasome complexes, 2) proteins that facilitate their activation (NLRP3, ASC, and Cleaved Caspase-1), and 3) end products of NLRP3 inflammasome activation (IL-1β and IL-18).

[Figure 4 here]

3.8. hiPSC-NSC-EVs diminished the activation of p38/MAPK signaling in the hippocampus

Since the end products of NLRP3 inflammasome activation (IL-1β and IL-18) and increased oxidative stress can mediate the downstream activation p38/MAPK inflammatory signaling cascade (Fig. 5 [A]), the proficiency of hiPSC-NSC-EVs to reduce the concentrations of proteins involved in p38/MAPK signaling activation (Myd88, Ras, pMAPK, AP-1) and some of the end products of p38/MAPK activation (TNF-α, IL-8) were measured (Fig, 5 [B-M]). Compared to the aged-Veh group, both males and females in the aged-EVs group displayed decreased concentrations of all measured proteins, with Myd88, Ras, pMAPK, AP-1, and TNF-α showing a significant decline in both sexes ($p<0.05$-0.001, Fig. 5 [B-F, H-L]). The concentration of IL-8 was significantly decreased in females ($p<0.05$, Fig. 5 [M]) but showed only a trend in males ($p=0.05$, Fig. 5 [G]). Two-way ANOVA analyses did not show sex-dependent differences in aged-Veh and aged-EVs groups for the concentrations of Myd88, Ras, AP-1, and IL-8 ($p>0.05$, Suppl. Table 1). The concentration of pMAPK displayed sex-specific differences, as its concentration was higher in females in the aged-EVs group ($p<0.05$, Suppl Table 1). The concentration of TNF-α also showed sex-specific differences because of the relatively higher concentration in the hippocampus of males in the aged-EVs group. However, post-hoc tests did not reveal significant differences (Suppl Table 1). Furthermore, no interaction was found between sex and hiPSC-NSC-EVs treatment for any of the proteins linked to p38/MAPK activation ($p>0.05$; Suppl Table 1). Thus, hiPSC-NSC-EV treatment in late middle-aged male and female mice prevented the activation of p38/MAPK inflammatory signaling in the aged hippocampus.

[Figure 5 here]

3.9. hiPSC-NSC-EVs curtailed the activation of cGAS-STING and the downstream JAK-STAT signaling in the hippocampus

As the cGAS–STING pathway is one of the drivers of aging-related inflammation in both peripheral organs and the brain [14], the ability of hiPSC-NSC-EVs to reduce the concentrations of proteins involved in cGAS-STING signaling activation (p-cGAS, p-STING, p-TBK1, p-IRF3) and one of its end product (IFN-α) were measured (Fig. 6 [A-J]). Compared to the aged-Veh group, both males and

females in the aged-EVs group displayed decreased concentrations of all measured proteins, with p-cGAS, p-STING, and p-IRF3, showing a significant decline in both sexes ($p<0.05$-0.01, Fig. 6 [A-B, D, F-G, I]). The concentration of p-TBK1 was significantly decreased in females ($p<0.0001$, Fig. 6 [H]) but showed only a trend in males ($p=0.058$, Fig. 6 [C]). The concentration of IFN-α was significantly decreased in males ($p<0.001$, Fig. 6 [E]) but showed only a trend in females ($p=0.0509$, Fig. 6 [J]). Two-way ANOVA analyses did not show sex-dependent differences in aged-Veh and aged-EVs groups for the concentrations of p-cGAS, p-STING, p-TBK1, and IFN-α ($p>0.05$, Suppl. Table 1). The concentration of p-IRF3 displayed sex-specific differences, as its concentration was higher in females in the aged-EVs group ($p<0.05$, Suppl Table 1). Furthermore, no interaction was found between sex and hiPSC-NSC-EVs treatment for most of the proteins linked to cGAS-STING activation ($p>0.05$; Suppl Table 1). The exception is the concentration of IFN-α, which showed an interaction between sex and EVs treatment, although both males and females responded positively to EVs treatment ($p<0.05$; Suppl Table 1). Thus, hiPSC-NSC-EVs treatment in late middle-age considerably diminished the activation of p38/MAPK inflammatory signaling in the hippocampus of both aged male and female mice.

Since increased release of IFN-α can lead to the activation of the downstream IFN-1 signaling through the JAK-STAT protein activation [45], the proficiency of hiPSC-NSC-EVs to reduce the concentrations of proteins involved in JAK-STAT signaling (p-JAK1, p-JAK2, p-STAT1, p-STAT3) were measured (Fig. 6 [K-R]). Compared to the aged-Veh group, both males and females in the aged-EVs group displayed significantly decreased concentrations of p-JAK2 and p-STAT1 ($p<0.05$, Fig. 6 [L-M, P-Q]). The concentration of p-JAK1 was significantly decreased in males ($p<0.01$, Fig. 6 [K]) but showed only a decreased trend in females ($p=0.056$, Fig. 6 [O]). The concentrations of p-STAT3 did not differ between aged-Veh and aged-EVs groups in both males and females (Fig. 6 [N, R). Two-way ANOVA analyses showed neither sex-dependent differences in aged-Veh and aged-EVs groups nor interactions between sex and hiPSC-NSC-EVs treatment for all measured proteins linked to JAK-STAT signaling ($p>0.05$, Suppl. Table 1). Thus, hiPSC-NSC-EVs treatment in late middle-age considerably diminished JAK-STAT activation involved in IFN-1 signaling in the hippocampus of both aged male and female mice.

[Figure 6 here]

3.10. hiPSC-NSC-EVs treatment in late middle-age led to improved cognitive function in old age

Recognition and object location memories were investigated respectively through a NORT (Fig. 7 [A]) and an OLT (Fig. 7 [J]). Animals proficient in recognition memory prefer to explore the novel object (NO) over the familiar object (FO). In contrast, animals competent for object location memory prefer to explore the object in the novel place (OINP) over the object in the familiar place (OIFP). We first confirmed that at the time point of hiPSC-NSC-EVs intervention, the strain of male and female mice chosen for the study do display recognition and object location memory impairments. These results obtained from separate cohorts of male and female mice are detailed in the Supplemental File (Suppl Fig. 1).

We next examined animals in aged-Veh and aged-EVs groups between 19.5 and 20.5 months of age (i.e., commencing one month after the last Veh/EVs treatment). Male and female mice receiving hiPSC-NSC-EVs treatment showed proficiency for both recognition and object location memories in NORT and OLT (Fig. 7 [A-R]). Representative tracings of the movement of mice from the aged-Veh and aged-EVs groups while exploring the FO and NO in trial-3 (T3) of a NORT or the OINP and OIFP in T3 of an OLT are illustrated (Fig. 7 [B-C, K-L]. In NORT, male and female mice in the aged-Veh group showed no preference to explore either the NO or the FO ($p>0.05$, Fig. 7 [D, G]), whereas male and female mice in the aged-EVs group preferred to explore the NO for longer durations than the FO ($p<0.001$, Fig. 7 [E, H]). In OLT, mice in the aged-Veh group showed a predilection for exploring the OIFP over the OINP ($p<0.01$-0.001, Fig. 7 [M, P]), whereas mice in the aged-EVs group exhibited a preference to explore the OINP for longer durations than the OIFP ($p<0.05$, Fig. 7 [N, Q]). Thus, male and female mice in the aged-Veh group displayed impairments in recognition and objection location memory formation. In contrast, male and female mice in the aged-EVs groups exhibited proficiency in recognition and objection location memory. Such conclusion is also confirmed by significantly lower NO/OINP-DI values in male and female mice in the aged-Veh group compared to their counterparts in the aged-EVs group ($p<0.05$-0.01; Fig. 7 [F, I, O, R]). Two-way ANOVA analyses showed neither sex-dependent differences in aged-Veh and aged-EVs groups nor interactions between sex and hiPSC-NSC-EVs treatment for NO or OINP-DI values in both NORT and OLT ($p>0.05$, Suppl. Table 1). Thus, hiPSC-NSC-EVs treatment in late middle age led to improved recognition and object location memory function in old age of both male and female mice.

[Figure 7 here]

4. DISCUSSION

The results provide the first evidence in a mouse model of aging that IN administrations of hiPSC-NSC-EVs in late middle age reduce oxidative stress and the activation of neuroinflammatory signaling cascades in the aged hippocampus and maintain improved cognitive function in old age. Remarkably, such anti-aging effects of hiPSC-NSC-EVs were seen in both male and female mice with no or minimal interaction of treatment with sex for various molecular and behavioral parameters.

4.1. Effect of hiPSC-NSC-EVs treatment on oxidative stress in the aged hippocampus

Increased oxidative stress is one of the characteristics of brain aging [10]. During brain aging, the levels of ROS rise steadily, and progressively increasing oxidative stress leads to mitochondrial dysfunction and synaptic oxidative damage in neurons [46]. Such changes contribute to age-related cognitive impairments and the progression of neurodegenerative diseases like AD [10]. Mitochondria, the powerhouses of cells, are the primary contributors to neuronal oxidative stress, as they generate most free radicals as byproducts of the mitochondrial electron transport chain. An accumulation of mitochondrial ROS can impair redox homeostasis and cause genomic instability, triggering the transcription of inflammatory genes and facilitating the release of proinflammatory cytokines such as IL-1β, IL-6, and TNF-α [10, 47]. Notably, increased ROS can damage or inactivate the elements of the electron transport chain in a positive feedback loop, leading to increased oxygen reduction into superoxide [47]. Investigations have also demonstrated that mitochondrial ROS can damage mitochondrial DNA (mtDNA), which in turn can impair nuclear DNA and neuronal function [10, 47-48].

Thus, strategies capable of mitigating oxidative stress and protecting the components of the electron transport chain can significantly prevent neuronal and cognitive dysfunction in old age.
In this context, the results of the current study are significant, as it demonstrated that hiPSC-NSC-EVs treatment in late-middle-aged male and female mice could effectively reduce oxidative stress and inactivation of the electron transport chain in the aged hippocampus. Such effect was apparent from significantly lower levels of MDA and PCs, indicators of oxidative stress-induced lipid peroxidation and protein oxidation, alongside elevated concentrations of NRF-2, a regulator of antioxidant defense, and SOD, a vital antioxidant enzyme, in male and female mice receiving hiPSC-NSC-EVs compared to their counterparts receiving the vehicle treatment. Besides, the expression of several genes encoding proteins

involved in maintaining the mitochondrial respiratory chain was normalized. While the specific mechanisms by which hiPSC-NSC-EVs mediate this protective effect against oxidative stress in the aged hippocampal microenvironment remain to be elucidated, one contributing factor may be the presence of hemopexin, a neuroprotective protein enriched in hiPSC-NSC-EVs used in this study [26]. Hemopexin is known for its ability to protect neurons from the harmful effects of heme and ROS through its heme oxygenase activity [49]. Additionally, reduced neuroinflammation mediated by hiPSC-NSC-EVs could have also contributed to lowering oxidative stress, as persistent neuroinflammation can increase oxidative stress in the neuronal microenvironment.

4.2. Impact of hiPSC-NSC-EVs on neuroinflammatory signaling cascades in the aged hippocampus

Age-related neuroinflammation, commonly referred to as inflammaging, is another hallmark of brain aging [50-51]. In the C57BL6 mice used in the study, the incidence of neuroinflammation escalates steadily as these mice age, accompanied by multiple alterations in microglia. Specifically, the aging microglia show increased proliferation rates, heightened reactivity, enhanced motility, and altered patterns of gene expression [52-54]. As part of the neuroinflammatory response, these inflammaging microglia express multiple proinflammatory markers, including IL-1β, TNF-α, IL-6, and major histocompatibility complex class II molecules [55], and release increased levels of proinflammatory cytokines [56]. These changes create a chronic inflammatory environment that is detrimental to neuronal function.

Furthermore, in the context of inflammaging, several key neuroinflammatory pathways are activated, significantly impacting the aging brain. The NLRP3 inflammasome pathway plays a critical role in this process [12-13]. The formation of NLRP3 inflammasome is triggered by DAMPs, such as elevated levels of ROS and cellular debris from dead neurons commonly found in the aging brain. The NLRP3 inflammasome is a multi-protein complex comprised of NLRP3, ASC, and procaspase-1 [15]. This complex activates caspase-1, which promotes the maturation of IL-1β and IL-18. Following their release, IL-1β and IL-18 initiate downstream signaling cascades, mainly through activating the p38/MAPK pathway. The process involves the activation of Myd88 and the small GTPase Ras, leading to the phosphorylation of MAPK followed by the transcription of AP-1. These events culminate in continuous release of multiple proinflammatory cytokines including IL-1β, IL-6, IL-8 and TNF-α and perpetuates chronic neuroinflammatory environment [12-13, 16-17]. Activation of the cGAS-STING-IFN-1 signaling is

the second pathway implicated in the neuroinflammatory processes observed in the aged brain [14]. The activation of this pathway, primarily triggered by the sensing of dsDNA or mtDNA [57], leads to a significant upregulation in the production of type I-IFNs, involved in antiviral defense and immune regulation [14, 17]. Subsequently, these interferons signal through the JAK-STAT pathway, which facilitates the transcription of interferon-stimulated genes (ISGs). Such process culminates in the promotion of IFN-1 signaling typified by neuroinflammatory processes and altered immune responses [14, 18, 58].

Thus, moderate but progressively increasing chronic neuroinflammation, backed by the activation of NLRP3-p38/MAPK and cGAS-STING-IFN-1 signaling in the brain, has emerged as a significant factor contributing to the cognitive decline observed with aging. Therefore, strategies that effectively target and reduce the activation of these neuroinflammatory signaling pathways are likely to maintain better cognitive function in old age. In this context, the current study's findings are significant, as they demonstrated that hiPSC-NSC-EVs treatment in late-middle-aged male and female mice resulted in a substantial reduction of chronic neuroinflammation within the aged hippocampus. The benefits of hiPSC-NSC-EVs treatment were evidenced through several beneficial alterations in the microglia and significant molecular changes within the hippocampal microenvironment. First, the treatment led to a marked decrease in the formation of microglial clusters and a decrease in the percentage of microglia exhibiting inflammasome complexes. Second, significant reductions in the concentrations of key proteins involved in activating the NLRP3 inflammasome and the p38/MAPK pathway were seen. These include NLRP3, ASC, cleaved Caspase-1, Myd88, Ras, pMAPK, and AP-1. Third, the treatment significantly lowered the levels of proteins involved in activating cGAS-STING-IFN-1 and JAK-STAT signaling cascades. These include notable reductions in p-cGAS, p-STING, p-IRF3, IFN-α, p-JAK1/2, and p-STAT1. These significant changes were consistent across male and female mice receiving the hiPSC-NSC-EVs treatment compared to their counterparts receiving vehicle treatment. Thus, hiPSC-NSC-EVs treatment in late middle age can slow down chronic neuroinflammation in the aged brain by restraining inflammatory signaling cascades.

4.3. Potential mechanisms by which hiPSC-NSC-EVs alleviated neuroinflammation in the aged hippocampus

The proficiency of hiPSC-NSC-EVs to restrain chronic neuroinflammatory signaling in the aged hippocampus observed in this study is unsurprising, as previous studies have documented the ability of these EVs to mediate robust antiinflammatory properties in multiple conditions. First, hiPSC-NSC-EVs have been shown to substantially decrease the release of IL-6 from lipopolysaccharide (LPS)-stimulated mouse macrophages and the release of IL-1β and TNF-α from LPS-stimulated hiPSC-derived iMicroglia [26, 28]. Second, in neuroinflammatory conditions induced by status epilepticus [26] or LPS-induced peripheral inflammation [29], hiPSC-NSC-EVs could substantially decrease neuroinflammation. Third, our recent study demonstrated that hiPSC-NSC-EVs intervention in the 3-month-old 5xFAD mice can modulate disease associated microglia and NLRP3-p38/MAPK and cGAS-STING-IFN-1 inflammatory signaling pathways without compromising their phagocytic activity of microglia [17]. The potential mechanisms by which hiPSC-NSC-EVs mediate antiinflammatory effects in the aged hippocampus could be gleaned from the miRNA and protein composition of hiPSC-NSC-EVs employed in this study. Small RNA sequencing and proteomic studies in our previous study have demonstrated that the cargo of hiPSC-NSC-EVs employed in this study comprises multiple miRNAs and proteins capable of promoting antiinflammatory effects [26]. Another study from our laboratory, by inhibition or knockdown approaches, has identified miR-21-5p and pentraxin-3 (PTX3) as potent antiinflammatory agents carried by hiPSC-NSC-EVs. Specifically, depleting miR-21-5p and PTX3 in hiPSC-NSC-EVs reduced their antiinflammatory effects on LPS-stimulated human iMicroglia [28]. miR-21-5p promotes antiinflammatory activity via multiple mechanisms, which include regulation of NF-kB signaling, increasing IL-10 levels, and inhibiting TNF-α release [59-62]. PTX3, on the other hand, has been shown to stimulate beneficial A2 astrocytes and preserve the blood-brain barrier [63-65]. Additionally, hiPSC-NSC-EVs are also enriched with miR-103a, capable of reducing neuroinflammation by inhibiting prostaglandin-endoperoxide synthase 2 [26, 66], hemopexin proficient in influencing the transformation of proinflammatory microglia into antiinflammatory microglia [67], and galectin-3 binding protein proficient in reducing NF-kB signaling pathway [68]. Thus, antiinflammatory effects mediated by hiPSC-NSC-EVS in the aged hippocampus of male and female mice observed in this study are likely a net effect of multiple miRNAs and proteins carried by these EVs.

4.4. Impact of hiPSC-NSC-EVs treatment in late middle age on cognitive function in old age

Cognitive and mood impairments are consistently observed in late middle-aged mice [69-71]. The current study also confirmed that at 18 months of age (i.e., the late middle-aged time point chosen

for hiPSC-NSC-EVs intervention in the study), male and female mice displayed memory impairments in two object-based tests. First, male and female mice exhibited recognition memory impairment in an NORT, a task in which mice failed to recognize a novel object, a memory function dependent on an appropriate interaction between the hippocampus and the perirhinal cortex [31]. Second, male and female mice could not form object location memory in an OLT, a task in which mice failed to perceive minor changes in their immediate environment, a cognitive function dependent on the integrity of the hippocampus [32]. Furthermore, the study found that recognition and object location memory impairments observed at 18 months of age persisted into old age for both male and female mice, as indicated by the performance of those receiving vehicle treatment. In contrast, male and female mice treated with hiPSC-NSC-EVs demonstrated proficiency in forming recognition and object location memories in old age. These findings imply that hiPSC-NSC-EVs treatment likely mediates beneficial molecular changes in the hippocampus and potentially also in other brain regions, leading to a reversal of cognitive impairments.

Increased oxidative stress and neuroinflammatory conditions are associated with cognitive impairments in late middle-aged and aged mice [72-75, 50]. Therefore, it is likely that the reduction of oxidative stress and the suppression of neuroinflammatory signaling pathways, facilitated by hiPSC-NSC-EVs treatment, have contributed to improving cognitive function in both male and female mice during old age. Such a conclusion is consistent with the fact that neuroinflammation is a significant risk factor for developing dementia, including AD [76]. However, there may be other beneficial changes induced by hiPSC-NSC-EVs that were not examined in this study, such as the impact of EVs on neurons, which have also contributed to improved cognitive function in aged male and female mice.

5. CONCLUSION

The results provide novel evidence that IN-administrations of hiPSC-NSC-EVs during late middle age can mediate sex-independent anti-aging effects in the hippocampus, leading to better cognitive function in older age. The observed anti-aging effects include sustained reductions in oxidative stress, microglial activation, astrocyte hypertrophy, and the activation of inflammatory signaling pathways such as NLRP3-p38/MAPK and cGAS-STING-IFN-1. Therefore, IN-administration of hiPSC-NSC-EVs shows promise as a wellness approach in middle age to prevent chronic neuroinflammation and the development of mild cognitive impairment and AD in old age.

ACKNOWLEDGEMENTS

The TEM images of hiPSC-NSC-EVs were taken at the Image Analysis Laboratory, Texas A&M Veterinary Medicine & Biomedical Sciences (RRIS: SCR_0222479).

DISCLOSURE STATEMENT

The authors declared no conflicts of interest.

DECLARATION OF GENERATIVE AI AND AI-ASSISTED TECHNOLOGIES IN THE WRITING PROCESS

During the preparation of this manuscript, the authors utilized the Grammarly software primarily to check Grammar and spelling but did not use AI-assisted technologies to generate manuscript text. The authors take full responsibility for the content of the publication.

AUTHOR CONTRIBUTIONS

Concept: AKS. Research design: AKS, LNM, MK, SR, SA, and RU. Data collection, analysis, and interpretation: LNM, MK, SR, SA, RU, GS, BS, YS, JEJ, PAS, XR, and AKS. Preparation of figure composites: LNM, MK, SR, SA and YS. Manuscript writing: LNM, MK, and AKS. All authors provided feedback, edits, and additions to the manuscript text and approved the final version of the manuscript.

ETHICAL APPROVAL

The animal care and experimental procedures were conducted per the animal protocol approved by the Animal Care and the Use Committee (IACUC) of Texas A&M University School of Medicine.

DATA AVAILABILITY

Source data are included in this original research article. Any additional data requests are available from the corresponding author upon request.

REFERENCES

1. Aunan JR, Cho WC, Soreide K. The Biology of Aging and Cancer: A Brief Overview of Shared and Divergent Molecular Hallmarks. Aging Dis. 2017;8(5):628-42.
2. de Magalhaes JP, Stevens M, Thornton D. The Business of Anti-Aging Science. Trends Biotechnol. 2017;35(11):1062-73.
3. Gurau F, Baldoni S, Prattichizzo F, Espinosa E, Amenta F, Procopio AD, et al. Anti-senescence compounds: A potential nutraceutical approach to healthy aging. Ageing Res Rev. 2018;46:14-31.
4. Stambler I. Recognizing Degenerative Aging as a Treatable Medical Condition: Methodology and Policy. Aging Dis. 2017;8(5):583-9.
5. Fan X, Wheatley EG, Villeda SA. Mechanisms of Hippocampal Aging and the Potential for Rejuvenation. Annu Rev Neurosci. 2017;40:251-72.
6. Bettio LEB, Rajendran L, Gil-Mohapel J. The effects of aging in the hippocampus and cognitive decline. Neurosci Biobehav Rev. 2017;79:66-86.
7. Turrini S, Wong B, Eldaief M, Press DZ, Sinclair DA, Koch G, et al. The multifactorial nature of healthy brain ageing: Brain changes, functional decline and protective factors. Ageing Res Rev. 2023;88:101939.
8. O'Shea A, Cohen RA, Porges EC, Nissim NR, Woods AJ. Cognitive Aging and the Hippocampus in Older Adults. Front Aging Neurosci. 2016;8:298.
9. Kodali M, Attaluri S, Madhu LN, Shuai B, Upadhya R, Gonzalez JJ, et al. Metformin treatment in late middle age improves cognitive function with alleviation of microglial activation and enhancement of autophagy in the hippocampus. Aging Cell. 2021;20(2):e13277.
10. Ionescu-Tucker A, Cotman CW. Emerging roles of oxidative stress in brain aging and Alzheimer's disease. Neurobiol Aging. 2021;107:86-95.
11. Bartman S, Coppotelli G, Ross JM. Mitochondrial Dysfunction: A Key Player in Brain Aging and Diseases. Curr Issues Mol Biol. 2024;46(3):1987-2026.
12. Fu Q, Li J, Qiu L, Ruan J, Mao M, Li S, Mao Q. Inhibiting NLRP3 inflammasome with MCC950 ameliorates perioperative neurocognitive disorders, suppressing neuroinflammation in the hippocampus in aged mice. Int Immunopharmacol. 2020;82:106317.
13. He XF, Li LL, Xian WB, Li MY, Zhang LY, Xu JH, et al. Chronic colitis exacerbates NLRP3-dependent neuroinflammation and cognitive impairment in middle-aged brain. J Neuroinflammation. 2021;18(1):153.
14. Gulen MF, Samson N, Keller A, Schwabenland M, Liu C, Gluck S, et al. cGAS-STING drives ageing-related inflammation and neurodegeneration. Nature. 2023;620(7973):374-80.
15. Ayyubova G, Madhu LN. Microglial NLRP3 Inflammasomes in Alzheimer's Disease Pathogenesis: From Interaction with Autophagy/Mitophagy to Therapeutics. Mol Neurobiol. 2025.
16. Kodali M, Madhu LN, Reger RL, Milutinovic B, Upadhya R, Gonzalez JJ, et al. Intranasally administered human MSC-derived extracellular vesicles inhibit NLRP3-p38/MAPK signaling after TBI and prevent chronic brain dysfunction. Brain Behav Immun. 2023;108:118-34.
17. Madhu LN, Kodali M, Upadhya R, Rao S, Somayaji Y, Attaluri S, et al. Extracellular vesicles from human-induced pluripotent stem cell-derived neural stem cells alleviate proinflammatory cascades within disease-associated microglia in Alzheimer's disease. J Extracell Vesicles. 2024;13(11):e12519.
18. Paul BD, Snyder SH, Bohr VA. Signaling by cGAS-STING in Neurodegeneration, Neuroinflammation, and Aging. Trends Neurosci. 2021;44(2):83-96.
19. Hedden T, Gabrieli JD. Insights into the ageing mind: a view from cognitive neuroscience. Nat Rev Neurosci. 2004;5(2):87-96.

20. Hattiangady B, Shuai B, Cai J, Coksaygan T, Rao MS, Shetty AK. Increased dentate neurogenesis after grafting of glial restricted progenitors or neural stem cells in the aging hippocampus. Stem Cells. 2007;25(8):2104-17.
21. Shetty AK, Hattiangady B. Grafted Subventricular Zone Neural Stem Cells Display Robust Engraftment and Similar Differentiation Properties and Form New Neurogenic Niches in the Young and Aged Hippocampus. Stem Cells Transl Med. 2016;5(9):1204-15.
22. Blurton-Jones M, Kitazawa M, Martinez-Coria H, Castello NA, Muller FJ, Loring JF, et al. Neural stem cells improve cognition via BDNF in a transgenic model of Alzheimer disease. Proc Natl Acad Sci U S A. 2009;106(32):13594-9.
23. Ager RR, Davis JL, Agazaryan A, Benavente F, Poon WW, LaFerla FM, Blurton-Jones M. Human neural stem cells improve cognition and promote synaptic growth in two complementary transgenic models of Alzheimer's disease and neuronal loss. Hippocampus. 2015;25(7):813-26.
24. Hattiangady B, Shetty AK. Neural stem cell grafting counteracts hippocampal injury-mediated impairments in mood, memory, and neurogenesis. Stem Cells Transl Med. 2012;1(9):696-708.
25. Eckert A, Huang L, Gonzalez R, Kim HS, Hamblin MH, Lee JP. Bystander Effect Fuels Human Induced Pluripotent Stem Cell-Derived Neural Stem Cells to Quickly Attenuate Early Stage Neurological Deficits After Stroke. Stem Cells Transl Med. 2015;4(7):841-51.
26. Upadhya R, Madhu LN, Attaluri S, Gitai DLG, Pinson MR, Kodali M, et al. Extracellular vesicles from human iPSC-derived neural stem cells: miRNA and protein signatures, and anti-inflammatory and neurogenic properties. J Extracell Vesicles. 2020;9(1):1809064.
27. Attaluri S, Jaimes Gonzalez J, Kirmani M, Vogel AD, Upadhya R, Kodali M, et al. Intranasally administered extracellular vesicles from human induced pluripotent stem cell-derived neural stem cells quickly incorporate into neurons and microglia in 5xFAD mice. Front Aging Neurosci. 2023;15:1200445.
28. Upadhya R, Madhu LN, Rao S, Shetty AK. Proficiency of Extracellular Vesicles From hiPSC-Derived Neural Stem Cells in Modulating Proinflammatory Human Microglia: Role of Pentraxin-3 and miRNA-21-5p. Front Mol Neurosci. 2022;15:845542.
29. Ayyubova G, Kodali M, Upadhya R, Madhu LN, Attaluri S, Somayaji Y, et al. Extracellular vesicles from hiPSC-NSCs can prevent peripheral inflammation-induced cognitive dysfunction with inflammasome inhibition and improved neurogenesis in the hippocampus. J Neuroinflammation. 2023;20(1):297.
30. Rao S, Madhu LN, Babu RS, Nagarajan A, Upadhya R, Narvekar E, Shetty AK. Extracellular Vesicles from hiPSC-derived NSCs Protect Human Neurons against Abeta-42 Oligomers Induced Neurodegeneration, Mitochondrial Dysfunction and Tau Phosphorylation. bioRxiv. 2024.
31. Aggleton JP, Albasser MM, Aggleton DJ, Poirier GL, Pearce JM. Lesions of the rat perirhinal cortex spare the acquisition of a complex configural visual discrimination yet impair object recognition. Behav Neurosci. 2010;124(1):55-68.
32. Barker GR, Warburton EC. When is the hippocampus involved in recognition memory? J Neurosci. 2011;31(29):10721-31.
33. Hattiangady B, Mishra V, Kodali M, Shuai B, Rao X, Shetty AK. Object location and object recognition memory impairments, motivation deficits and depression in a model of Gulf War illness. Front Behav Neurosci. 2014;8:78.
34. Shetty AK, Attaluri S, Kodali M, Shuai B, Shetty GA, Upadhya D, et al. Monosodium luminol reinstates redox homeostasis, improves cognition, mood and neurogenesis, and alleviates neuro- and systemic inflammation in a model of Gulf War Illness. Redox Biol. 2020;28:101389.
35. Rao MS, Hattiangady B, Shetty AK. Status epilepticus during old age is not associated with enhanced hippocampal neurogenesis. Hippocampus. 2008;18(9):931-44.

36. Hattiangady B, Kuruba R, Shetty AK. Acute Seizures in Old Age Leads to a Greater Loss of CA1 Pyramidal Neurons, an Increased Propensity for Developing Chronic TLE and a Severe Cognitive Dysfunction. Aging Dis. 2011;2(1):1-17.
37. Rao MS, Hattiangady B, Shetty AK. Fetal hippocampal CA3 cell grafts enriched with FGF-2 and BDNF exhibit robust long-term survival and integration and suppress aberrant mossy fiber sprouting in the injured middle-aged hippocampus. Neurobiol Dis. 2006;21(2):276-90.
38. Rao MS, Hattiangady B, Rai KS, Shetty AK. Strategies for promoting anti-seizure effects of hippocampal fetal cells grafted into the hippocampus of rats exhibiting chronic temporal lobe epilepsy. Neurobiol Dis. 2007;27(2):117-32.
39. Kodali M, Megahed T, Mishra V, Shuai B, Hattiangady B, Shetty AK. Voluntary Running Exercise-Mediated Enhanced Neurogenesis Does Not Obliterate Retrograde Spatial Memory. J Neurosci. 2016;36(31):8112-22.
40. Madhu LN, Kodali M, Attaluri S, Shuai B, Melissari L, Rao X, Shetty AK. Melatonin improves brain function in a model of chronic Gulf War Illness with modulation of oxidative stress, NLRP3 inflammasomes, and BDNF-ERK-CREB pathway in the hippocampus. Redox Biol. 2021;43:101973.
41. Chen M, Yu S, van der Sluis T, Zwager MC, Schroder CP, van der Vegt B, van Vugt M. cGAS-STING pathway expression correlates with genomic instability and immune cell infiltration in breast cancer. NPJ Breast Cancer. 2024;10(1):1.
42. Silvin A, Uderhardt S, Piot C, Da Mesquita S, Yang K, Geirsdottir L, et al. Dual ontogeny of disease-associated microglia and disease inflammatory macrophages in aging and neurodegeneration. Immunity. 2022;55(8):1448-65 e6.
43. Antignano I, Liu Y, Offermann N, Capasso M. Aging microglia. Cell Mol Life Sci. 2023;80(5):126.
44. Stefanatos R, Sanz A. The role of mitochondrial ROS in the aging brain. FEBS Lett. 2018;592(5):743-58.
45. Raftery N, Stevenson NJ. Advances in anti-viral immune defence: revealing the importance of the IFN JAK/STAT pathway. Cell Mol Life Sci. 2017;74(14):2525-35.
46. Grimm A, Eckert A. Brain aging and neurodegeneration: from a mitochondrial point of view. J Neurochem. 2017;143(4):418-31.
47. Islam MT. Oxidative stress and mitochondrial dysfunction-linked neurodegenerative disorders. Neurol Res. 2017;39(1):73-82.
48. Lu T, Pan Y, Kao SY, Li C, Kohane I, Chan J, Yankner BA. Gene regulation and DNA damage in the ageing human brain. Nature. 2004;429(6994):883-91.
49. Hahl P, Davis T, Washburn C, Rogers JT, Smith A. Mechanisms of neuroprotection by hemopexin: modeling the control of heme and iron homeostasis in brain neurons in inflammatory states. J Neurochem. 2013;125(1):89-101.
50. Britton R, Liu AT, Rege SV, Adams JM, Akrapongpisak L, Le D, et al. Molecular and histological correlates of cognitive decline across age in male C57BL/6J mice. Brain Behav. 2022;12(9):e2736.
51. Mosher KI, Wyss-Coray T. Microglial dysfunction in brain aging and Alzheimer's disease. Biochem Pharmacol. 2014;88(4):594-604.
52. Long JM, Kalehua AN, Muth NJ, Calhoun ME, Jucker M, Hengemihle JM, et al. Stereological analysis of astrocyte and microglia in aging mouse hippocampus. Neurobiol Aging. 1998;19(5):497-503.
53. Harry GJ. Microglia during development and aging. Pharmacol Ther. 2013;139(3):313-26.
54. Hefendehl JK, Neher JJ, Suhs RB, Kohsaka S, Skodras A, Jucker M. Homeostatic and injury-induced microglia behavior in the aging brain. Aging Cell. 2014;13(1):60-9.
55. Wolf SA, Boddeke HW, Kettenmann H. Microglia in Physiology and Disease. Annu Rev Physiol. 2017;79:619-43.

56. Yu WH, Go L, Guinn BA, Fraser PE, Westaway D, McLaurin J. Phenotypic and functional changes in glial cells as a function of age. Neurobiol Aging. 2002;23(1):105-15.
57. Jimenez-Loygorri JI, Villarejo-Zori B, Viedma-Poyatos A, Zapata-Munoz J, Benitez-Fernandez R, Frutos-Lison MD, et al. Mitophagy curtails cytosolic mtDNA-dependent activation of cGAS/STING inflammation during aging. Nat Commun. 2024;15(1):830.
58. Baruch K, Deczkowska A, David E, Castellano JM, Miller O, Kertser A, et al. Aging. Aging-induced type I interferon response at the choroid plexus negatively affects brain function. Science. 2014;346(6205):89-93.
59. Ge X, Huang S, Gao H, Han Z, Chen F, Zhang S, et al. miR-21-5p alleviates leakage of injured brain microvascular endothelial barrier in vitro through suppressing inflammation and apoptosis. Brain Res. 2016;1650:31-40.
60. Sheedy FJ. Turning 21: Induction of miR-21 as a Key Switch in the Inflammatory Response. Front Immunol. 2015;6:19.
61. Slota JA, Booth SA. MicroRNAs in Neuroinflammation: Implications in Disease Pathogenesis, Biomarker Discovery and Therapeutic Applications. Noncoding RNA. 2019;5(2).
62. Barnett RE, Conklin DJ, Ryan L, Keskey RC, Ramjee V, Sepulveda EA, et al. Anti-inflammatory effects of miR-21 in the macrophage response to peritonitis. J Leukoc Biol. 2016;99(2):361-71.
63. Shindo A, Maki T, Mandeville ET, Liang AC, Egawa N, Itoh K, et al. Astrocyte-Derived Pentraxin 3 Supports Blood-Brain Barrier Integrity Under Acute Phase of Stroke. Stroke. 2016;47(4):1094-100.
64. Rajkovic I, Wong R, Lemarchand E, Tinker R, Allan SM, Pinteaux E. Pentraxin 3 regulates neutrophil infiltration to the brain during neuroinflammation. AMRC Open Res. 2019;1:10.
65. Zhou C, Chen H, Zheng JF, Guo ZD, Huang ZJ, Wu Y, et al. Pentraxin 3 contributes to neurogenesis after traumatic brain injury in mice. Neural Regen Res. 2020;15(12):2318-26.
66. Yang H, Wang H, Shu Y, Li X. miR-103 Promotes Neurite Outgrowth and Suppresses Cells Apoptosis by Targeting Prostaglandin-Endoperoxide Synthase 2 in Cellular Models of Alzheimer's Disease. Front Cell Neurosci. 2018;12:91.
67. Han D, Yu Z, Liu W, Yin D, Pu Y, Feng J, et al. Plasma Hemopexin ameliorates murine spinal cord injury by switching microglia from the M1 state to the M2 state. Cell Death Dis. 2018;9(2):181.
68. Seki T, Kanagawa M, Kobayashi K, Kowa H, Yahata N, Maruyama K, et al. Galectin 3-binding protein suppresses amyloid-beta production by modulating beta-cleavage of amyloid precursor protein. J Biol Chem. 2020;295(11):3678-91.
69. Frick KM, Burlingame LA, Arters JA, Berger-Sweeney J. Reference memory, anxiety and estrous cyclicity in C57BL/6NIA mice are affected by age and sex. Neuroscience. 2000;95(1):293-307.
70. Barreto G, Huang TT, Giffard RG. Age-related defects in sensorimotor activity, spatial learning, and memory in C57BL/6 mice. J Neurosurg Anesthesiol. 2010;22(3):214-9.
71. Radulescu CI, Cerar V, Haslehurst P, Kopanitsa M, Barnes SJ. The aging mouse brain: cognition, connectivity and calcium. Cell Calcium. 2021;94:102358.
72. Morrison JH, Baxter MG. The ageing cortical synapse: hallmarks and implications for cognitive decline. Nat Rev Neurosci. 2012;13(4):240-50.
73. Petralia RS, Mattson MP and Yao PJ. Communication breakdown: the impact of ageing on synapse structure. Ageing Res Rev. 2014;14:31-42.
74. Bhatt DH, Zhang S, Gan WB. Dendritic spine dynamics. Annu Rev Physiol. 2009;71:261-82.
75. Holtmaat A, Svoboda K. Experience-dependent structural synaptic plasticity in the mammalian brain. Nat Rev Neurosci. 2009;10(9):647-58.
76. Walker KA, Le Page LM, Terrando N, Duggan MR, Heneka MT, Bettcher BM. The role of peripheral inflammatory insults in Alzheimer's disease: a review and research roadmap. Mol Neurodegener. 2023;18(1):37.

FIGURE LEGENDS

Figure 1: ***Characterization of extracellular vesicles (EVs) from human induced pluripotent stem cell-derived neural stem cells (hiPSC-NSCs), assessment of hiPSC-NSC-EVs biodistribution in the hippocampus and cerebral cortex of late middle-aged mice, and timeline of in vivo experiments.*** Image A illustrates that all cells in the passage 11 NSCs derived from hiPSCs express NSC markers Nestin and Sox-2. Graph B shows the size and number of hiPSC-NSC-EVs measured with a NanoSight. The blots in C demonstrate EV-specific proteins CD63, CD81, and ALIX and the absence of the deep cellular protein calnexin in hiPSC-NSC-EVs. The image in D display the morphology and size of hiPSC-NSC-EVs visualized through transmission electron microscopy. scale bars, A=100 µm, D=50nm. Panel E illustrates the experimental design for assessing the biodistribution of hiPSC-NSC-EVs in late middle-aged male mice. Figure F illustrates the incorporation of EVs into IBA-1+ microglia in different hippocampal subregions (DG, CA1, CA3). Figure G illustrates the incorporation of EVs into GFAP+ astrocytes in hippocampal subregions (DG, CA1, CA3). Scale bar, F-G =10 µm. Panel H illustrates the experimental design showing the time points of hiPSC-NSC-EVs treatment, cognitive and mood function tests, euthanasia, and brain tissue harvest in late middle-aged male and female mice.

Figure 2: ***Intranasal administration of extracellular vesicles from human induced pluripotent stem cell-derived neural stem cells (hiPSC-NSC-EVs) to late middle-aged mice reduced hypertrophy of astrocytes and microglial clusters.*** Figures A-D illustrate the representative images of GFAP+ astrocytes in aged-Veh (A, C) and aged-EVs (B, D) for males (A-B) and females (C-D). Bar charts E-F compare the area fraction (AF) of GFAP+ structures in the hippocampus of males (E) and females (F) between the aged-Veh and aged-EV groups. Figures G-J illustrate the representative images of IBA-1+ microglia in aged-Veh (G, I) and aged-EVs (H, J) for males (G-H) and females (I-J). Bar charts K-L compare the density of IBA-1+ microglia per 0.1 mm^3 in the hippocampus of males (K) and females (L) between the aged-Veh and aged-EV groups. Figures M-P illustrate the representative images of microglia clusters in aged-Veh (M, O) and aged-EVs (N, P) for males (M-N) and females (O-P). Bar charts Q-R compare the number of microglia clusters in the hippocampus of males (Q) and females (R) between the aged-Veh and aged-EV groups. Scale bar, A-D, G-J, M-P = 25 µm **, $p<0.01$; ***, $p<0.001$; and ****, $p<0.0001$.

Figure 3: ***Intranasal administration of extracellular vesicles from human induced pluripotent stem cell-derived neural stem cells (hiPSC-NSC-EVs) to late middle-aged mice reduced oxidative stress and***

normalized the mitochondrial respiratory chain gene expression. The bar charts A-J compare malondialdehyde (A, F), protein carbonyl (B, G), NRF-2 (C, H), SOD (D, I), and catalase (E, J) between aged-Veh and aged-EVs groups in males (A-E) and females (F-J). Heatmaps K and V compare the expression of multiple mitochondrial respiratory chain genes between aged-Veh and aged-EV groups in male (K) and female (V) mice. Bar charts L-U (male), and W-AF (female) show the relative expression of genes Ndufs6 (L, W), Ndufs7 (M, X), Sdha (N, Y), Sdhb (O, Z), Cyc1 (P, AA), Bcs1l (Q, AB), Cox7b (R, AC), Cox4i2 (S, AD), Slc25a1 (T, AE) and Atp6ap1 (U, AF) in aged-Veh and aged-EV groups. *, $p<0.05$; **, $p<0.01$; ***, $p<0.001$; ****, $p<0.0001$.

Figure 4: ***Intranasal administration of extracellular vesicles from human induced pluripotent stem cell-derived neural stem cells (hiPSC-NSC-EVs) to late middle-aged mice inhibited NOD-, LRR- and pyrin domain-containing protein 3 (NLRP3) and apoptosis-associated speck-like protein containing a CARD (ASC) inflammasome complex formation.*** Heatmaps A and G compare the expression of multiple NLRP3 inflammasome genes between aged-Veh and aged-EV groups in male (A) and female (G) mice. The bar charts B-F, H-L compare nlrp3 (B, H), pycard (C, I), casp1 (D, J), IL-18 (E, K) and IL-1β (F, L) across aged-Veh and aged-EVs groups in males (B-F) and females (H-L). Figures M-Y- illustrate examples of NLRP3 inflammasome complexes co-expressing NLRP3 (green) and ASC (red) in IBA-1+ microglia (blue) in the CA3 subfield of the hippocampus from male (M-R) and female (T-Y) mice belonging to aged-Veh (M-O, T-V) and aged-EVs (P-R, W-Y) groups. The bar charts S and Z compare the percentages of microglia with inflammasome complexes in males (S) and females (Z). The bar graphs AA-AL compare the concentrations of different proteins involved in the activation of NLRP3 inflammasomes, such as NF-kB p65 (AA, AG), NLRP3 (AB, AH), ASC (AC, AI), cleaved caspase-1 (AD, AJ), IL-18 (AE, AK), and IL-1β (AF, AL) between aged-Veh and aged-EVs groups of male (AA-AF) and female (AG-AL) mice. M-Y = 25 µm; *, $p<0.05$; **, $p<0.01$; ***, $p<0.001$; ****, $p<0.0001$.

Figure 5: ***Intranasal administration of extracellular vesicles from human induced pluripotent stem cell-derived neural stem cells (hiPSC-NSC-EVs) to late middle-aged mice inhibited p38/mitogen-activated protein kinase (p38/MAPK) signaling.*** Figure A is a cartoon depicting the mechanisms by which the activation of MAPK signaling occurs in the aged brain. The bar charts in B-M compare the concentrations of p38MAPK signaling-related proteins between aged-Veh and aged-EVs groups in male and female mice. The proteins include Myd88 (B, H), Ras (C, I), p38/MAPK (D, J), transcription factor AP-1 (E, K), and

end products such as TNF-α (F, L) and IL-8 (G, M) in male (B-G) and female (H-M) mice. *, $p<0.05$; **, $p<0.01$; ***, $p<0.001$.

Figure 6: ***Intranasal administration of extracellular vesicles from human induced pluripotent stem cell-derived neural stem cells (hiPSC-NSC-EVs) to late middle-aged mice inhibited cGAS-STING and JAK-STAT pathway activation.*** The bar charts A-J compare the concentration of proteins linked to cGAS-STING pathway, such as p-total cGAS (A, F), p-STING (B, G), p-TBK1 (C, H), p-IRF3 (D, I), and IFN-α (E, J) in males (A-E) and females (F-J). The bar charts K-R compare the concentration of proteins linked to the JAK-STAT pathway, such as p-JAK1 (K, O), p-JAK2 (L, P), p-STAT1 (M, Q), and p-STAT3 (N, R) in male (K-N) and female (O-R) mice. *, $p<0.05$; **, $p<0.01$; ***, $p<0.001$; ****, $p<0.0001$.

Figure 7: ***Intranasal administration of extracellular vesicles from human induced pluripotent stem cell-derived neural stem cells (hiPSC-NSC-EVs) to late middle-aged mice improved cognitive dysfunction.*** Cartoon A depicts different trials (T1-T3) in a novel object recognition test (NORT). The representative tracings in B-C illustrate the exploration of objects by male mice for aged-Veh (B) and aged-EVs groups (C) in T3. The bar charts in D-E and G-H compare percentages of object exploration times spent with the familiar object (FO) vis-à-vis the novel object (NO) in aged-Veh (D, G) and aged-EV groups (E, H) in males (D-E) and Females (G-H). The bar charts F and I compare the NO discrimination index for males (F) and females (I). Cartoon J depicts different trials (T1-T3) in an object location test (OLT). The representative tracings in K-L illustrate the exploration of objects by female mice for aged-Veh (K) and aged-EVs groups (L) in T3. The bar charts in M-N and P-Q compare percentages of object exploration times spent object with the familiar place (OIFP) vis-à-vis the object in the novel place (OINP) in aged-Veh (M, P) and aged-EV groups (N, Q) in males (M-N) and Females (P-Q). The bar charts O and R compare the OINP discrimination index for males (O) and females (R). *, $p<0.05$; **, $p<0.01$; ***, $p<0.001$.

Figure 1

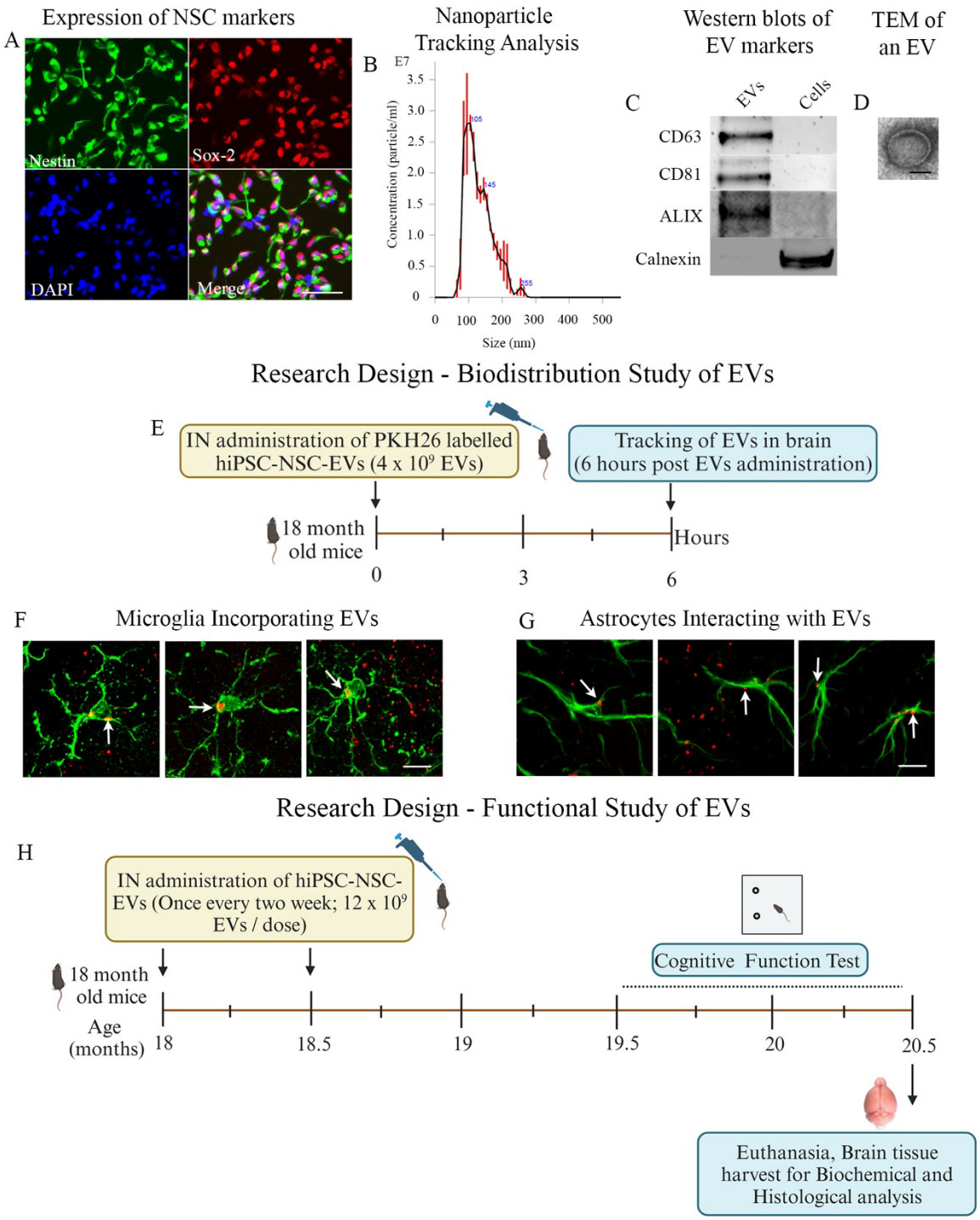

Figure 1: ***Characterization of extracellular vesicles (EVs) from human induced pluripotent stem cell-derived neural stem cells (hiPSC-NSCs), assessment of hiPSC-NSC-EVs biodistribution in the***

hippocampus and cerebral cortex of late middle-aged mice, and timeline of in vivo experiments. Image A illustrates that all cells in the passage 11 NSCs derived from hiPSCs express NSC markers Nestin and Sox-2. Graph B shows the size and number of hiPSC-NSC-EVs measured with a NanoSight. The blots in C demonstrate EV-specific proteins CD63, CD81, and ALIX and the absence of the deep cellular protein calnexin in hiPSC-NSC-EVs. The image in D display the morphology and size of hiPSC-NSC-EVs visualized through transmission electron microscopy. scale bars, A=100 µm, D=50nm. Panel E illustrates the experimental design for assessing the biodistribution of hiPSC-NSC-EVs in late middle-aged male mice. Figure F illustrates the incorporation of EVs into IBA-1+ microglia in different hippocampal subregions (DG, CA1, CA3). Figure G illustrates the incorporation of EVs into GFAP+ astrocytes in hippocampal subregions (DG, CA1, CA3). Scale bar, F-G =10 µm. Panel H illustrates the experimental design showing the time points of hiPSC-NSC-EVs treatment, cognitive and mood function tests, euthanasia, and brain tissue harvest in late middle-aged male and female mice.

Figure 2

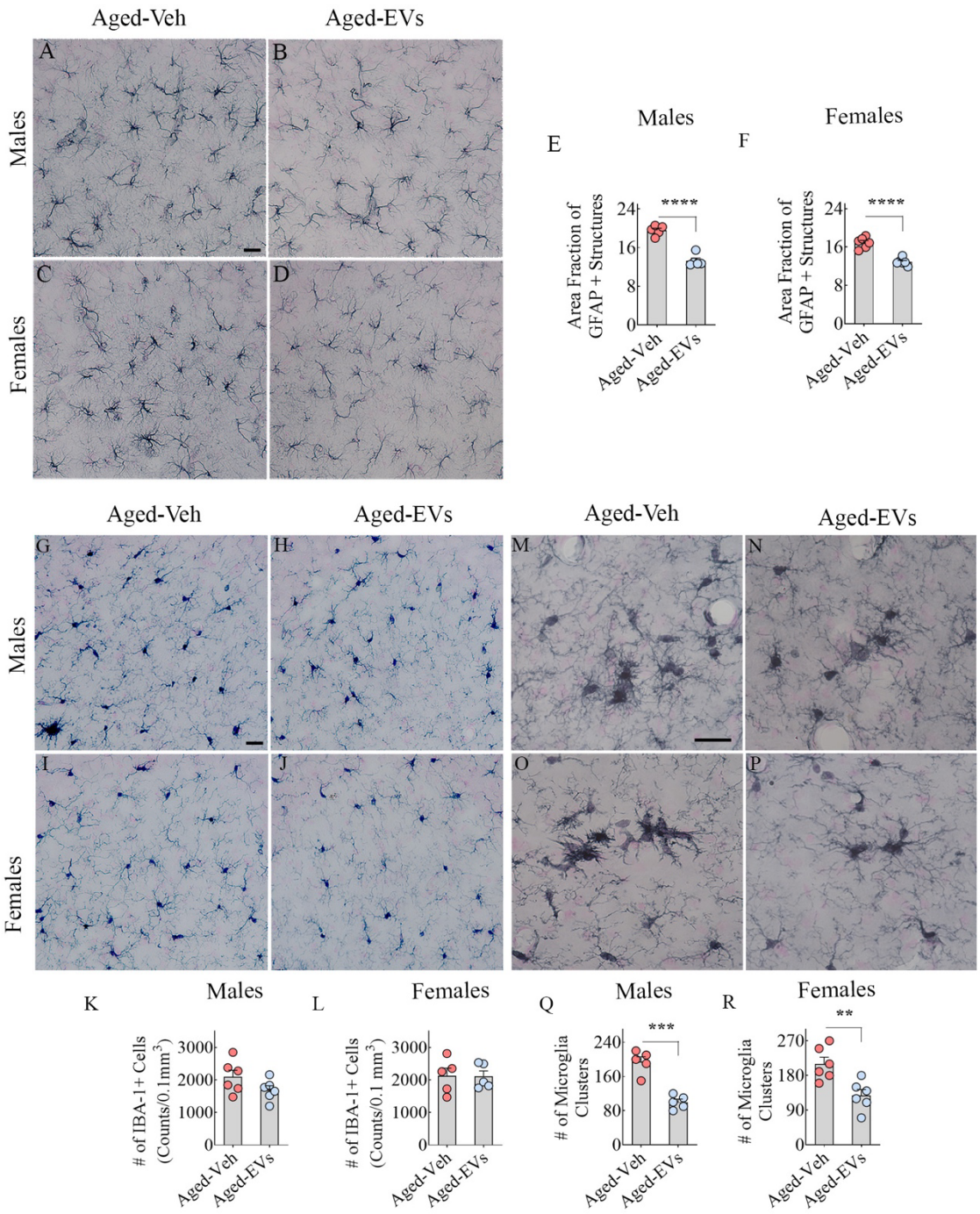

Figure 2: ***Intranasal administration of extracellular vesicles from human induced pluripotent stem cell-derived neural stem cells (hiPSC-NSC-EVs) to late middle-aged mice reduced hypertrophy of astrocytes and microglial clusters.*** Figures A-D illustrate the representative images of GFAP+ astrocytes in aged-

Veh (A, C) and aged-EVs (B, D) for males (A-B) and females (C-D). Bar charts E-F compare the area fraction (AF) of GFAP+ structures in the hippocampus of males (E) and females (F) between the aged-Veh and aged-EV groups. Figures G-J illustrate the representative images of IBA-1+ microglia in aged-Veh (G, I) and aged-EVs (H, J) for males (G-H) and females (I-J). Bar charts K-L compare the density of IBA-1+ microglia per 0.1 mm^3 in the hippocampus of males (K) and females (L) between the Aged-Veh and aged-EV groups. Figures M-P illustrate the representative images of microglia clusters in aged-Veh (M, O) and aged-EVs (N, P) for males (M-N) and females (O-P). Bar charts Q-R compare the number of microglia clusters in the hippocampus of males (Q) and females (R) between the aged-Veh and aged-EV groups. Scale bar, A-D, G-J, M-P = 25 µm **, $p<0.01$; ***, $p<0.001$; and ****, $p<0.0001$.

Figure 3

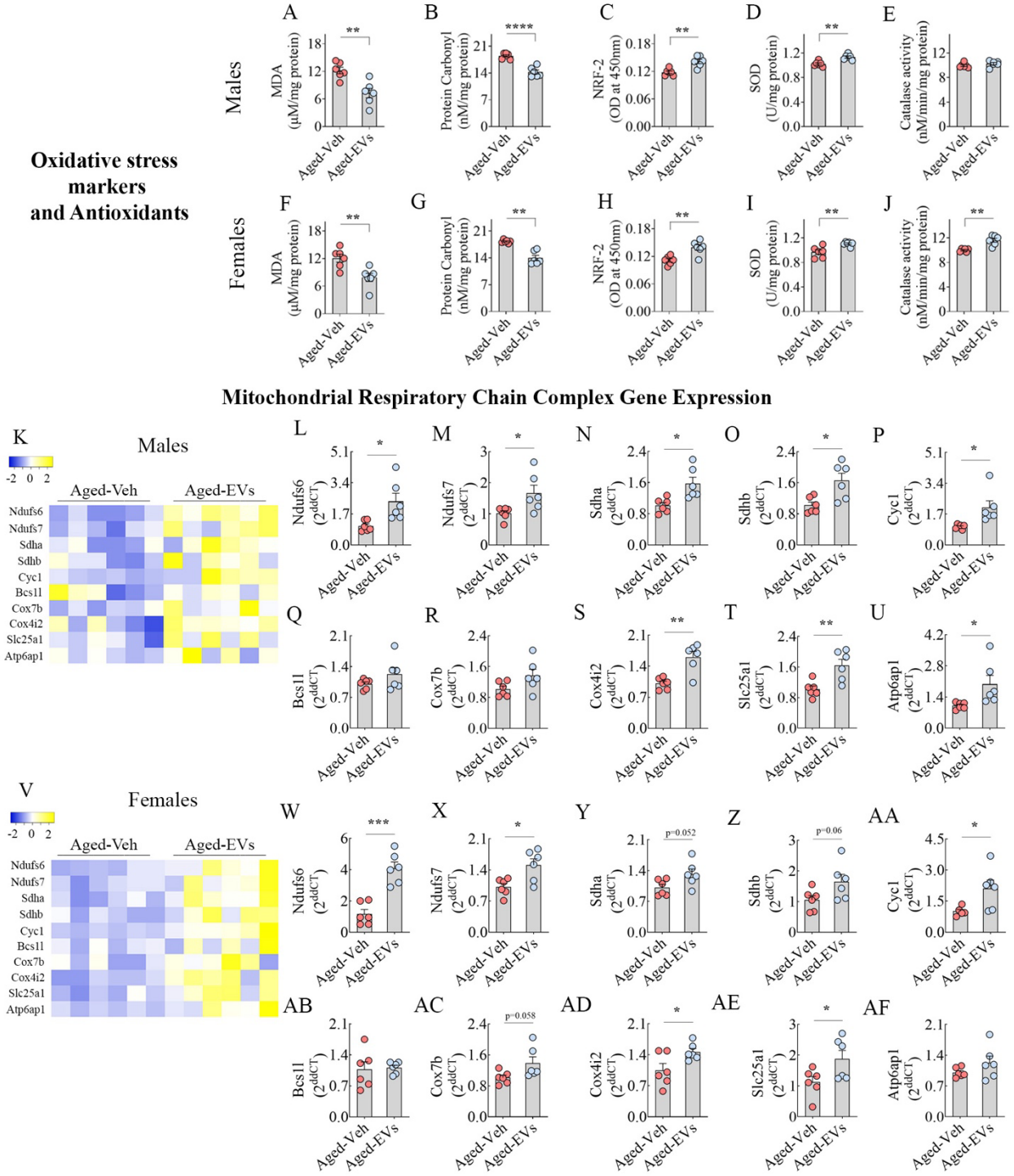

Figure 3: ***Intranasal administration of extracellular vesicles from human induced pluripotent stem cell-derived neural stem cells (hiPSC-NSC-EVs) to late middle-aged mice reduced oxidative stress and normalized the mitochondrial respiratory chain gene expression.*** The bar charts A-J compare

malondialdehyde (A, F), protein carbonyl (B, G), NRF-2 (C, H), SOD (D, I), and catalase (E, J) between aged-Veh and aged-EVs groups in males (A-E) and females (F-J). Heatmaps K and V compare the expression of multiple mitochondrial respiratory chain genes between aged-Veh and aged-EV groups in male (K) and female (V) mice. Bar charts L-U (male), and W-AF (female) show the relative expression of genes Ndufs6 (L, W), Ndufs7 (M, X), Sdha (N, Y), Sdhb (O, Z), Cyc1 (P, AA), Bcs1l (Q, AB), Cox7b (R, AC), Cox4i2 (S, AD), Slc25a1 (T, AE) and Atp6ap1 (U, AF) in aged-Veh and aged-EV groups. *, $p<0.05$; **, $p<0.01$; ***, $p<0.001$; ****, $p<0.0001$.

Figure 4

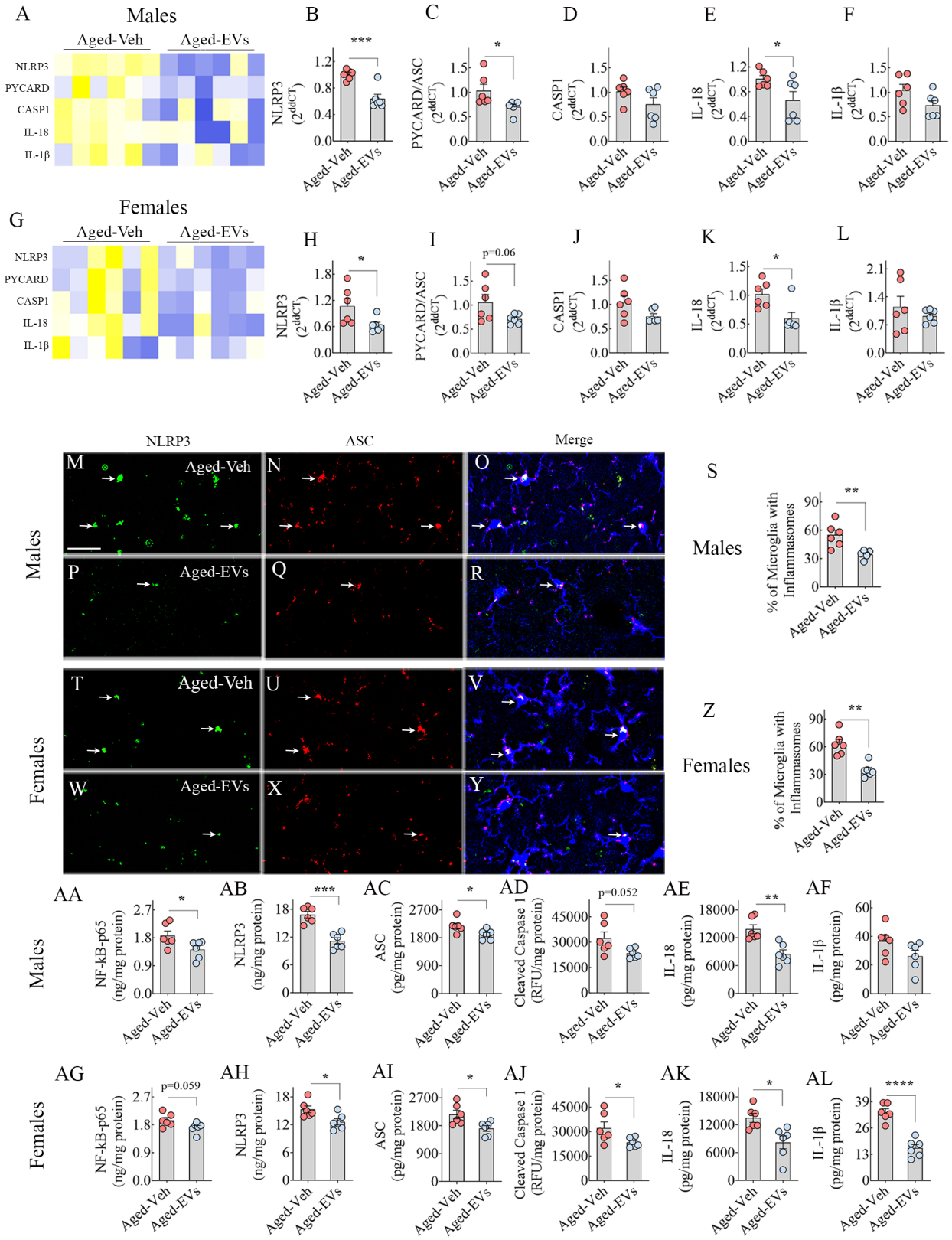
A
Males
Aged-Veh
Aged-EVs
NLRP3
PYCARD
CASP1
IL-18
IL-1β
B
C
D
E
F
NLRP3 (2^ddCT)
PYCARD/ASC (2^ddCT)
CASP1 (2^ddCT)
IL-18 (2^ddCT)
IL-1β (2^ddCT)
G
Females
H
I
J
K
L
p=0.06
NLRP3
ASC
Merge
M
N
O
P
Q
R
S
Males
% of Microglia with Inflammasomes
T
U
V
W
X
Y
Z
Females
AA
AB
AC
AD
AE
AF
NF-kB-p65 (ng/mg protein)
NLRP3 (ng/mg protein)
ASC (pg/mg protein)
Cleaved Caspase 1 (RFU/mg protein)
IL-18 (pg/mg protein)
IL-1β (pg/mg protein)
p=0.052
AG
AH
AI
AJ
AK
AL
p=0.059

Figure 4: ***Intranasal administration of extracellular vesicles from human induced pluripotent stem cell-derived neural stem cells (hiPSC-NSC-EVs) to late middle-aged mice inhibited NOD-, LRR- and pyrin domain-containing protein 3 (NLRP3) and apoptosis-associated speck-like protein containing a CARD (ASC) inflammasome complex formation.*** Heatmaps A and G compare the expression of multiple NLRP3 inflammasome genes between aged-Veh and aged-EV groups in male (A) and female (G) mice. The bar charts B-F, H-L compare nlrp3 (B, H), pycard (C, I), casp1 (D, J), IL-18 (E, K) and IL-1β (F, L) across aged-Veh and aged-EVs groups in males (B-F) and females (H-L). Figures M-Y- illustrate examples of NLRP3 inflammasome complexes co-expressing NLRP3 (green) and ASC (red) in IBA-1+ microglia (blue) in the CA3 subfield of the hippocampus from male (M-R) and female (T-Y) mice belonging to aged-Veh (M-O, T-V) and aged-EVs (P-R, W-Y) groups. The bar charts S and Z compare the percentages of microglia with inflammasome complexes in males (S) and females (Z). The bar graphs AA-AL compare the concentrations of different proteins involved in the activation of NLRP3 inflammasomes, such as NF-kB p65 (AA, AG), NLRP3 (AB, AH), ASC (AC, AI), cleaved caspase-1 (AD, AJ), IL-18 (AE, AK), and IL-1β (AF, AL) between aged-Veh and aged-EVs groups of male (AA-AF) and female (AG-AL) mice. M-Y = 25 µm; *, $p<0.05$; **, $p<0.01$; ***, $p<0.001$; ****, $p<0.0001$.

Figure 5

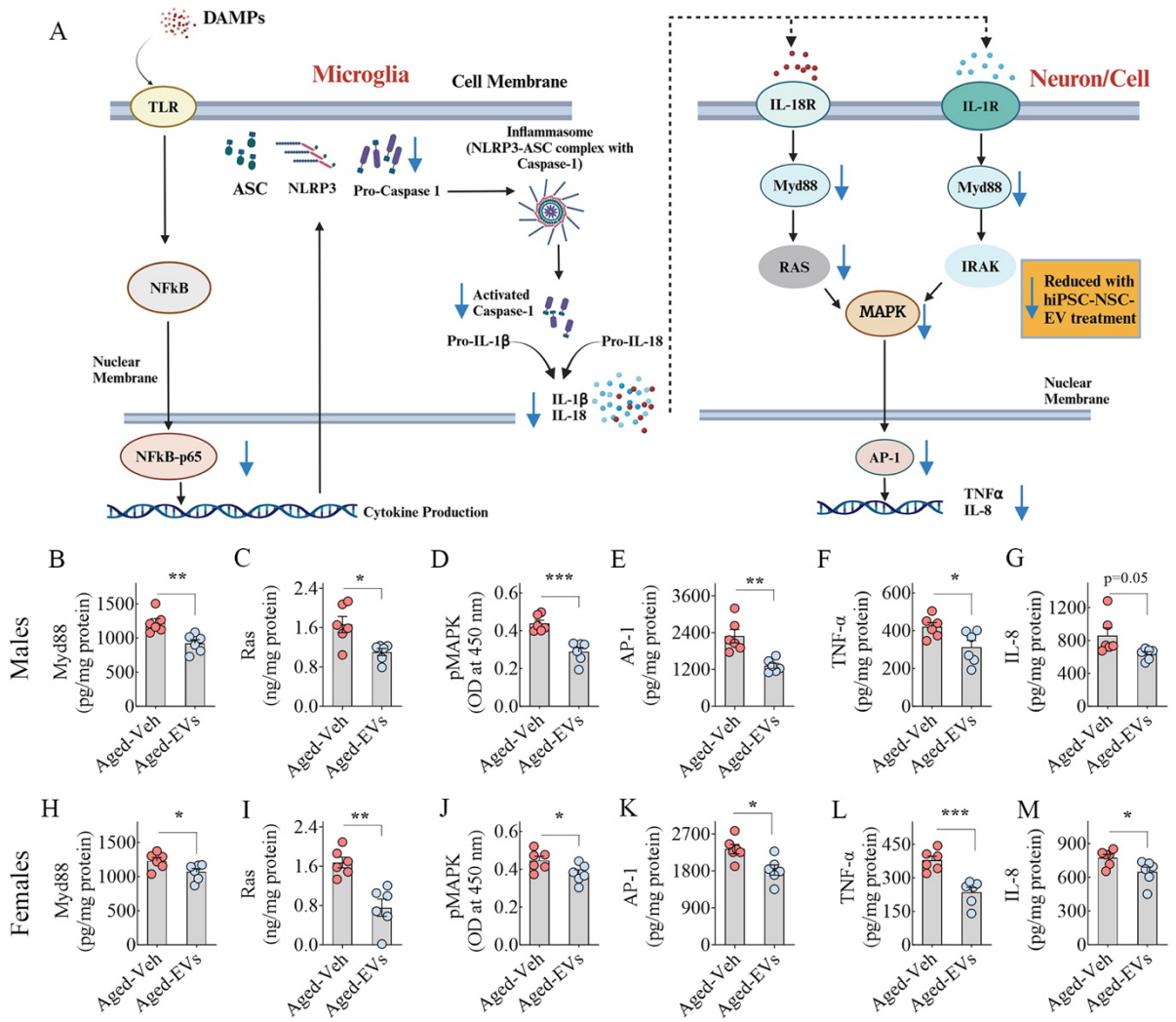

Figure 5: ***Intranasal administration of extracellular vesicles from human induced pluripotent stem cell-derived neural stem cells (hiPSC-NSC-EVs) to late middle-aged mice inhibited p38/mitogen-activated protein kinase (p38/MAPK) signaling.*** Figure A is a cartoon depicting the mechanisms by which the activation of MAPK signaling occurs in the aged brain. The bar charts in B-M compare the concentrations of p38MAPK signaling-related proteins between aged-Veh and aged-EVs groups in male and female mice. The proteins include Myd88 (B, H), Ras (C, I), p38/MAPK (D, J), transcription factor AP-1 (E, K), and end products such as TNF-α (F, L) and IL-8 (G, M) in male (B-G) and female (H-M) mice. *, $p<0.05$; **, $p<0.01$; ***, $p<0.001$.

Figure 6

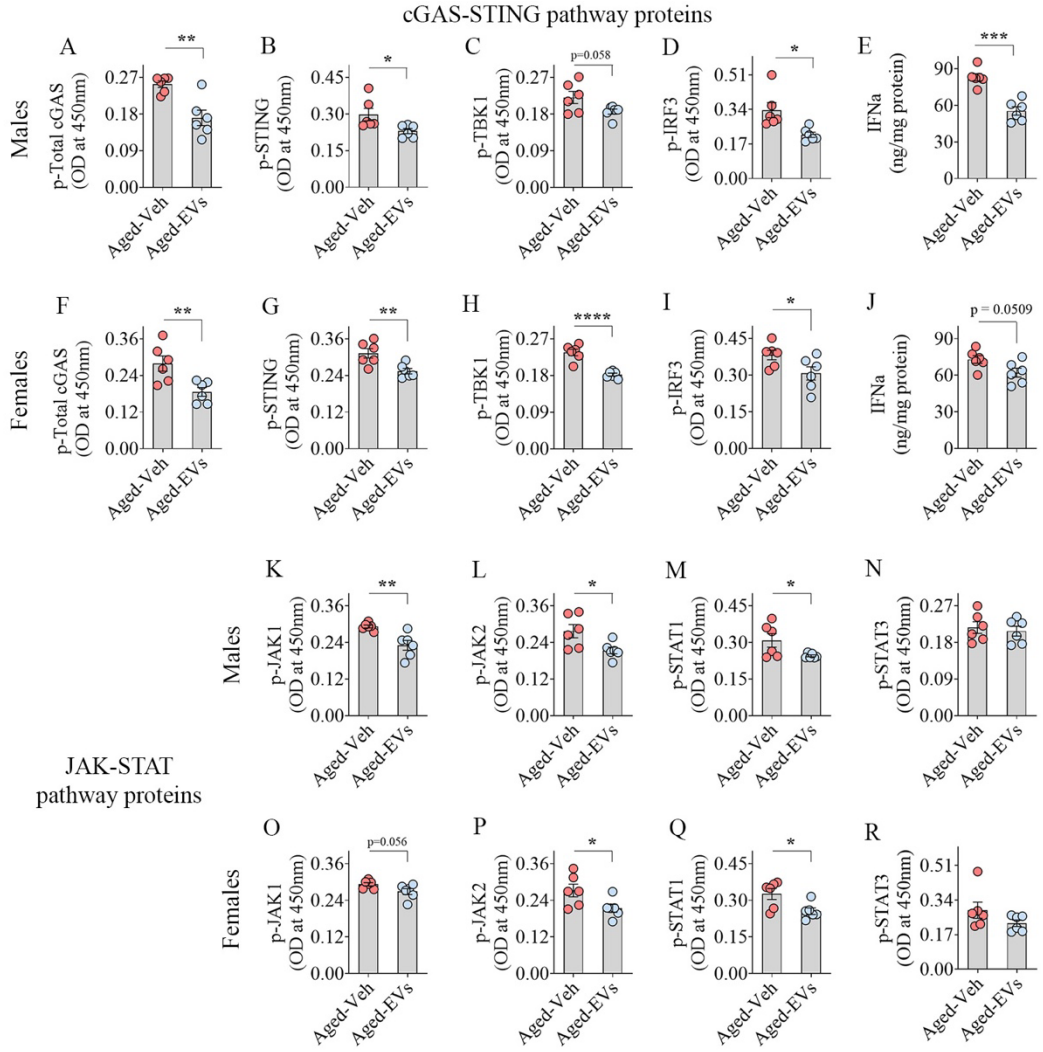

Figure 6: ***Intranasal administration of extracellular vesicles from human induced pluripotent stem cell-derived neural stem cells (hiPSC-NSC-EVs) to late middle-aged mice inhibited cGAS-STING and JAK-STAT pathway activation.*** The bar charts A-J compare the concentration of proteins linked to cGAS-STING pathway, such as p-total cGAS (A, F), p-STING (B, G), p-TBK1 (C, H), p-IRF3 (D, I), and IFN-α (E, J) in males (A-E) and females (F-J). The bar charts K-R compare the concentration of proteins linked to the JAK-STAT pathway, such as p-JAK1 (K, O), p-JAK2 (L, P), p-STAT1 (M, Q), and p-STAT3 (N, R) in male (K-N) and female (O-R) mice. *, p<0.05; **, p<0.01; ***, p<0.001; ****, p<0.0001.

Figure 7

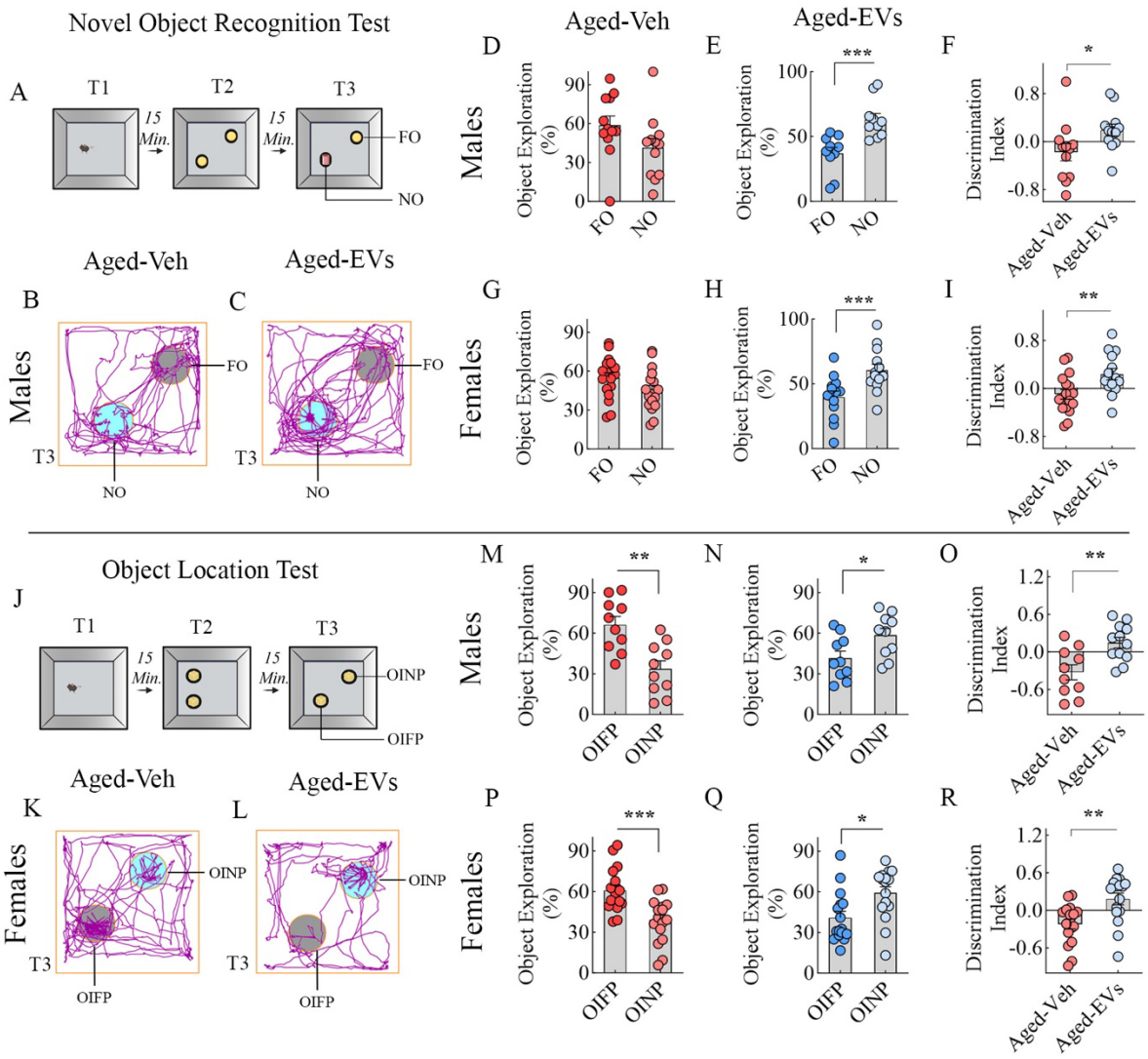

Figure 7: ***Intranasal administration of extracellular vesicles from human induced pluripotent stem cell-derived neural stem cells (hiPSC-NSC-EVs) to late middle-aged mice improved cognitive dysfunction.*** Cartoon A depicts different trials (T1-T3) in a novel object recognition test (NORT). The representative tracings in B-C illustrate the exploration of objects by male mice for aged-Veh (B) and aged-EVs groups (C) in T3. The bar charts in D-E and G-H compare percentages of object exploration times spent with the familiar object (FO) vis-à-vis the novel object (NO) in aged-Veh (D, G) and aged-EV groups (E, H) in males (D-E) and Females (G-H). The bar charts F and I compare the NO discrimination index for males (F) and females (I). Cartoon J depicts different trials (T1-T3) in an object location test (OLT). The representative tracings in K-L illustrate the exploration of objects by female mice for aged-Veh (K) and aged-EVs groups (L) in T3. The bar charts in M-N and P-Q compare percentages of object exploration times spent object with the familiar place (OIFP) vis-à-vis the object in the novel place (OINP) in aged-Veh (M, P) and aged-EV groups (N, Q) in males (M-N) and Females (P-Q). The bar charts O

and R compare the OINP discrimination index for males (O) and females (R). *, $p<0.05$; **, $p<0.01$; ***, $p<0.001$.